



Geophysical-petrological modeling of the lithosphere beneath the Cantabrian Mountains and the North-Iberian margin: geodynamic implications

David Pedreira ^{a,*}, Juan Carlos Afonso ^b, Javier A. Pulgar ^a, Jorge Gallastegui ^a, Alberto Carballo ^c, Manel Fernàndez ^c, Daniel Garcia-Castellanos ^c, Ivone Jiménez-Munt ^c, Julia Semprich ^{d,1}, Olga García-Moreno ^a

^a Departamento de Geología, Universidad de Oviedo, Oviedo, Spain

^b CCFS-Department of Earth and Planetary Sciences, Macquarie University, Sydney, Australia

^c Institute of Earth Sciences “Jaume Almera”, CSIC, Barcelona, Spain

^d Physics of Geological Processes, University of Oslo, Norway

ARTICLE INFO

Article history:

Received 19 August 2014

Accepted 23 April 2015

Available online 9 May 2015

Keywords:

Cantabrian Mountains

North-Iberian margin

Pyrenees

Geophysical-petrological modeling

Lithosphere

Mantle exhumation

ABSTRACT

Cenozoic contractional deformation in the North-Iberian continental margin (southern Bay of Biscay) led to the uplift of the Cantabrian Mountains and the northward subduction of part of the thick continental crust, down to at least ~55 km depth beneath the coastline, and perhaps even ~30–40 km deeper. In order to provide a more constrained model of this unique structure and gain insight into the factors controlling its evolution, we performed an integrated geophysical-petrological modeling of the lithosphere along a 470 km-long, N-S transect down to 400 km depth. The methodology used allows for fitting gravity anomalies, geoid undulations, surface heat flow, elevation and seismic velocities with a realistic distribution of densities and seismic velocities in the mantle and the subducting lower crust, which are dependent on chemical composition, pressure and temperature. Two models are presented, with variable maximum depth for the crustal root: 60 km (Model A) and 90 km (Model B). Results indicate that both models are feasible from the geophysical point of view, but the shallower root agrees slightly better with tomographic results. The thickness of the thermal lithosphere in Model A varies from 125–145 km south of the Cantabrian Mountains to 170 km beneath the crustal root and 135–140 km beneath the central part of the Bay of Biscay. Model B requires a thicker thermal lithosphere beneath the crustal root (205 km). Low seismic velocities beneath the Bay of Biscay Moho and in the mantle wedge above the crustal root are explained by the addition of 1–2 wt% of water. Input from dehydration reactions in the subducting lower crust is ruled out in Model A and has a very minor influence in Model B. We therefore interpret the water to have percolated from the seafloor during the formation of the margin in the Mesozoic. A later basaltic underplating was also inferred. A tentative evolutionary model (to a great extent governed by these petrological processes) is proposed, implying a minimum shortening close to 100 km from the Latest Cretaceous to the present.

© 2015 Elsevier B.V. All rights reserved.

1. Introduction

Passive margins and mountain belts are among the most relevant tectonic features on Earth, and are intimately related through the “Wilson cycle” of plate creation and destruction (Wilson, 1966). Rifting processes within continents may result in the formation of passive margins, which may later evolve into convergent margins

creating either collisional or non-collisional orogens. Recently, significant progress was made toward the understanding of the processes governing the formation and evolution of rifted margins, including the key role of structural inheritance, thermal and rheological stratification of the lithosphere and divergence velocity, among others (eg. Huisman and Beaumont, 2007, 2011; Manatschal et al., 2015; Pérez-Gussinyé and Reston, 2001). However, much less effort has been focused on the effects that the structure and composition of passive margins have on their subsequent tectonic inversion and their control on the architecture of mountain belts (eg. Jammes et al., 2014; Tugend et al., 2014).

The North-Iberian (or Cantabrian) continental margin and the Cantabrian Mountains in northern Spain (Fig. 1) are especially interesting to study these relationships for several reasons. First, the North-

* Corresponding author at: Departamento de Geología, Universidad de Oviedo, C/J. Arías de Velasco, s/n, 33005 Oviedo, Spain.

E-mail address: david@geol.uniovi.es (D. Pedreira).

¹ Now at Department of Geology and Natural Resources, Institute of Geosciences, University of Campinas, Brazil.

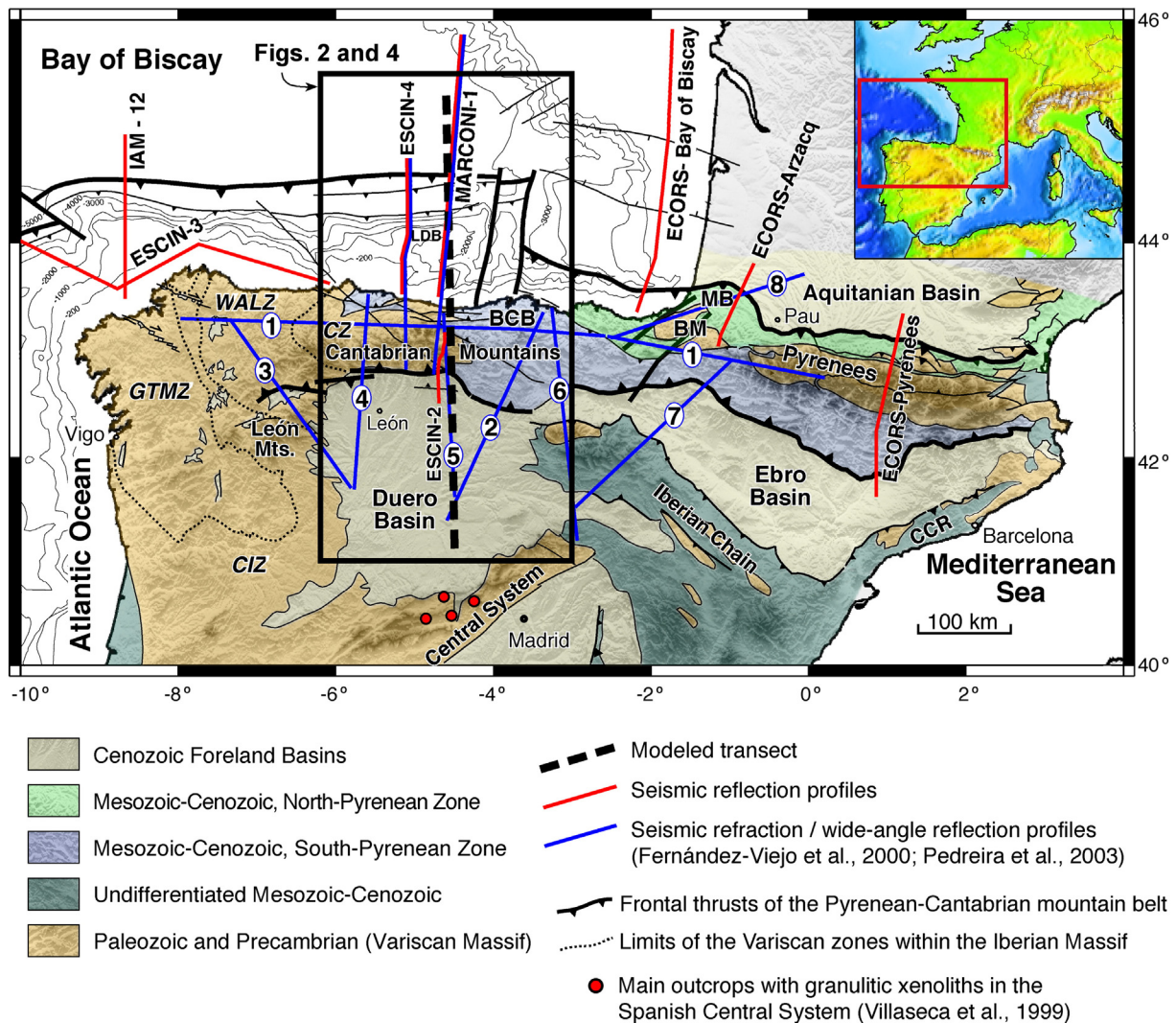


Fig. 1. Tectonic map of the Pyrenean-Cantabrian mountain belt in North-Iberia showing the location of the modeled N-S lithospheric transect and available deep seismic profiles. BCB, Basque-Cantabrian basin; BM, Basque Massifs; CCR, Catalan Coastal Ranges; MB, Mauléon basin. Acronyms in italics refer to tectonometamorphic zones within the Iberian Variscan Massif: CIZ, Central Iberian Zone; CZ, Cantabrian Zone; GTMZ, Galicia – Tras os Montes Zone; WALZ, West Asturian-Leonese Zone.

Iberian margin is a rare example of a margin that evolved from passive to convergent after only ~45 my of post-rift history, being one of the shortest-lived examples of passive margins worldwide (Bradley, 2008). It formed during the opening of the Bay of Biscay in the Mesozoic, and was soon affected by the convergence between the Iberian and European plates during the latest Cretaceous-Cenozoic in the framework of the Alpine orogeny. Second, its convergent stage was also aborted at an early stage of development, so that the passive margin structure can be well constrained. This is also facilitated by a good geophysical dataset available in the area. The convergent stage is also peculiar because it led to the subduction of the thickest (inner) part of the margin toward the outer margin, at the same time as the Cantabrian Mountains were uplifted from the former continental platform. The north-directed crustal root (the same polarity as in the Pyrenees) is located approximately beneath the present-day shoreline, which adds further interest to this area from the isostatic point of view.

To understand how and to which extent the particular configuration of such a young passive margin conditioned its later evolution under a convergent setting, we need a well-constrained model of the structural,

thermal, geochemical and petrophysical architecture of the crust and upper mantle.

Despite the good geological and geophysical knowledge of this area, several key issues are still poorly known. One of these issues is the nature of the basement beneath the margin. The oceanic crust with undoubtedly oceanic magnetic anomalies is present only approximately to the west of the meridian of 6°W, the remaining part of the margin being composed of thinned continental or “transitional” crust (Gallastegui et al., 2002; Roca et al., 2011; Ruiz, 2007; Sibuet et al., 2004). Seismic velocity-depth profiles in this ocean-continent transition reveal a high-velocity lower crust (~7.20–7.30 km s⁻¹) on top of a low-velocity upper mantle (~7.7–7.9 km s⁻¹) (Fernández-Viejo et al., 1998; Gallart et al., 1997; Ruiz, 2007). These velocities can be explained either by upper mantle hydration/serpentinization (eg. Roca et al., 2011) and/or by magma addition at the base of the crust by decompression melting during lithospheric thinning, but the relative importance of these processes remains enigmatic. This has important implications on the style of the tectonic inversion, because these two processes produce very different modifications in the rheological profile of the lithosphere.

Another unknown is the maximum depth of the crustal root and the effects that eclogitization/dehydration reactions have on the isostatic equilibrium and on the hydration of the overlying mantle wedge during the evolution of the tectonic convergence. The crustal root is well imaged by seismic methods down to at least 50–55 km depth beneath the central part of the Cantabrian Mountains (Fernández-Viejo et al., 1998; Gallastegui, 2000; Gallastegui et al., 2002; Pedreira et al., 2003, 2007; Pulgar et al., 1996). Seismic data, however, do not preclude a deeper root. In this sense, the balancing of a N-S crustal transect across this area proposed by Gallastegui (2000) requires that the Iberian lower crust reaches ~90 km depth. Obtaining a geophysical image of such a deep root is a difficult task because the density and seismic velocities of eclogitized lower crust are close to those of the surrounding mantle. The modeling of geoid undulations is useful in this case, as they are more sensitive to deeper (more distant) density differences than gravity anomalies. This is because gravitational potential is inversely proportional to the distance d from the source masses, whereas gravitational acceleration is inversely proportional to d^2 .

Geoid undulations are also very sensitive to lateral changes in lithospheric thickness and thermal and compositional anomalies in the mantle, which in turn have strong effects on the surface heat flow and elevation. Including these observables in the modeling allows us to estimate the topography of the thermal lithosphere-asthenosphere boundary (LAB), which is also poorly constrained in the area. A previous attempt following this type of combined approach was made by Ayarza et al. (2004), but along a N-S transect to the west, following the meridian of 7°W, where the crustal root is much less developed. In their study, the density of the lithospheric mantle was considered to decrease with depth as the temperature increases (neglecting the effect of pressure) and the density of the sublithospheric mantle was regarded as constant. Pedreira et al. (2010) presented a preliminary 3D model of the Cantabrian Mountains fitting also gravity anomalies and geoid undulations, but in this case the densities of both the lithospheric and sublithospheric mantle were assumed to be constant.

In this paper we apply a more realistic approach using the finite-element code LitMod (Afonso et al., 2008) to model the 2D lithospheric structure of the Cantabrian mountains and continental margin. The studied transect is 470 km-long, N-S oriented approximately following the meridian of 4.5°W, and down to 400 km depth. Densities and isotropic P-wave velocities in the mantle and the subducting Iberian lower crust are computed by the code according to their pressure-temperature conditions and assigned chemical compositions (cf. Afonso et al., 2008; Connolly, 2009). For the remaining crustal bodies, densities are assumed to be constant. A forward modeling scheme is then applied to simultaneously fit gravity anomalies, geoid undulations, surface heat flow, elevation (assuming local isostasy or some degree of flexural support) and P-wave velocities. Calculated seismic velocities are compared with those retrieved from seismic profiles and tomographic models. In this way we can test the feasibility of specific compositions for the lower crust and mantle and track the metamorphic reactions taking place, including dehydration/hydration reactions with important rheological implications. Petrology is therefore implicitly incorporated into the geophysical modeling.

The aim of this study is to obtain a more reliable model of the lithospheric structure of the North-Iberian margin and the Cantabrian Mountains, using geophysical and petrological constraints, and to draw conclusions on the processes operating during the formation and inversion of this margin. Specific targets are: (1) to constrain the composition, size and degree of densification of the crustal root; (2) to explore the possible relationship between dehydration/eclogitization of the root and hydration of the overlying mantle wedge; (3) to determine the composition and thickness of the lithospheric mantle; and (4) to explore the range of scenarios that may explain the particular distribution of seismic velocities observed between the lower crust and the upper mantle in the continental margin, providing an evolutionary model coherent with all the observations.

2. Geological setting

The Cantabrian Mountains are located immediately south of the northern coastline of the Iberian Peninsula. They are limited to the south by the Tertiary Duero basin and its connection with the Ebro basin (Fig. 1). This belt shows the imprints of three major tectonic events during the Phanerozoic. The oldest one is the Variscan Orogeny, which resulted from the collision of Laurussia with Gondwana between the Late Devonian and the late Carboniferous (Matte, 1991; Pérez-Estaún et al., 1991). Paleozoic and Precambrian rocks deformed by this tectonic event crop out along the central and western parts of the Cantabrian Mountains, forming part of the Variscan Iberian Massif. General vergences are to the east, but the structural trends are complicated by the later development of the Cantabrian Orocline in the latest Carboniferous (eg. Gutiérrez Alonso et al., 2012). Four zones of the Iberian Massif are recognized in the Cantabrian Mountains (Farias et al., 1987; Julivert et al., 1972) (Fig. 1); from E to W: 1) The Cantabrian Zone (CZ), representing the foreland fold-and-thrust belt; 2) the West Asturian-Leonese Zone (WALZ), characterized by pervasive internal deformation and increasing metamorphic degree (up to amphibolite facies) toward the west; 3) the Central-Iberian Zone (CIZ), corresponding to the most internal part of the orogen, with abundance of granitic rocks; and 4) the Galicia-Tras os Montes Zone (GTMZ), comprising parautochthonous and allochthonous units, including ophiolitic and catanzonal rocks.

The Variscan orogenic edifice was soon eroded, and after short rifting pulses in the Permian and Triassic, the second major tectonic event developed gradually in the area. It corresponds to a long period of lithospheric extension related to the opening of the Central Atlantic. Starting in the Late Jurassic, the new rifting stage gave rise to an array of sedimentary basins between Iberia and Eurasia, with the thickest troughs located around the present-day tip of the Bay of Biscay: the Parentis, Basque-Cantabrian and Mauléon basins. To the west, lithospheric extension led to the formation of passive margins (the North-Iberian or Cantabrian margin and its conjugate to the north, the Armorican margin). This process culminated in the mid to Late Cretaceous with seafloor spreading in the axis of the Bay of Biscay, with clear oceanic crust magnetic anomalies only to the west of ~6°W (eg. Sibuet et al., 2004).

The Basque-Cantabrian basin (BCB) holds several thousand meters of sediments deposited during this second event in the area presently occupied by the eastern Cantabrian Mountains (Fig. 1). Post-rift subsidence in this basin started in the late Albian and was coeval with intermittent but persistent alkaline volcanic activity that lasted up to the Santonian (Azambre and Rossy, 1976; Castañares et al., 2001). The western limit of the Basque-Cantabrian basin was a rather diffuse transfer zone between the meridians of 3.75°–4°W (Santander-Torrelavega Transfer Zone (Pedreira et al., 2007; Roca et al., 2011)). West of this boundary, the depocenter was slightly shifted northward, to the Le Danois basin, located in the present-day continental platform (Fig. 2). During the Late Cretaceous, however, the sediments of the Le Danois basin were deposited in the continental slope of the margin (Boillot et al., 1979). A thin succession of distal fluvial sandstones and shallow water carbonates of this age are presently outcropping to the south of the coastline (Fig. 2), unconformably overlying the Variscan basement in the Cantabrian Zone and beneath the Tertiary deposits of the Duero foreland basin (Alonso et al., 1996).

The last major tectonic event began in the Campanian, when the northward drift of the African plate forced the convergence between Iberia and Eurasia in the context of the Alpine orogeny. As a result, the Mesozoic basins were inverted and the Pyrenean-Cantabrian mountain belt developed as a doubly-vergent orogen all along north Iberia, mainly during the Tertiary. This mountain belt shows remarkable along-strike differences in the style of crustal deformation, but the northward subduction of the Iberian crust is a shared feature from east to west (Muñoz, 2002; Pedreira et al., 2003, 2007; Pulgar et al., 1996).

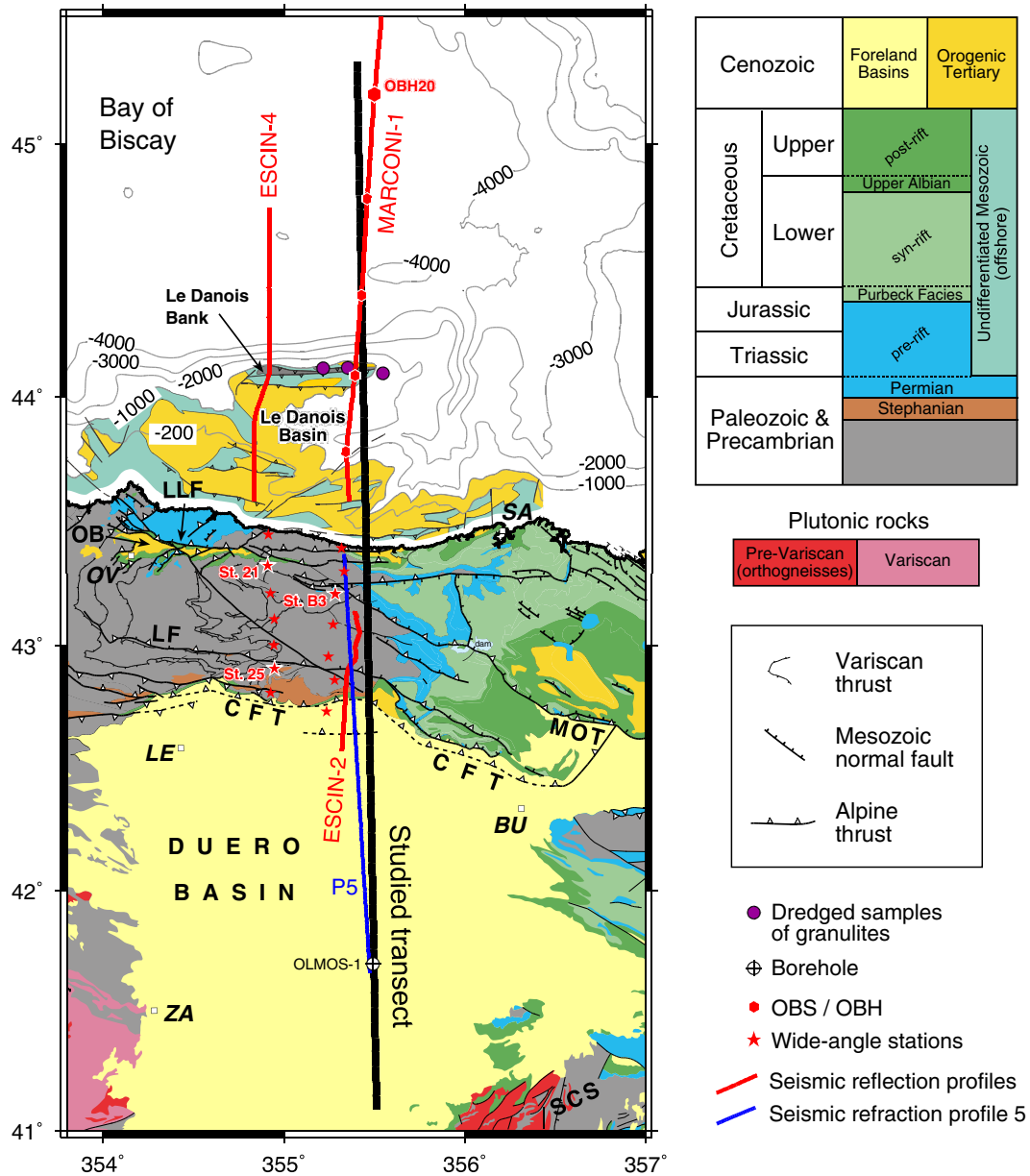
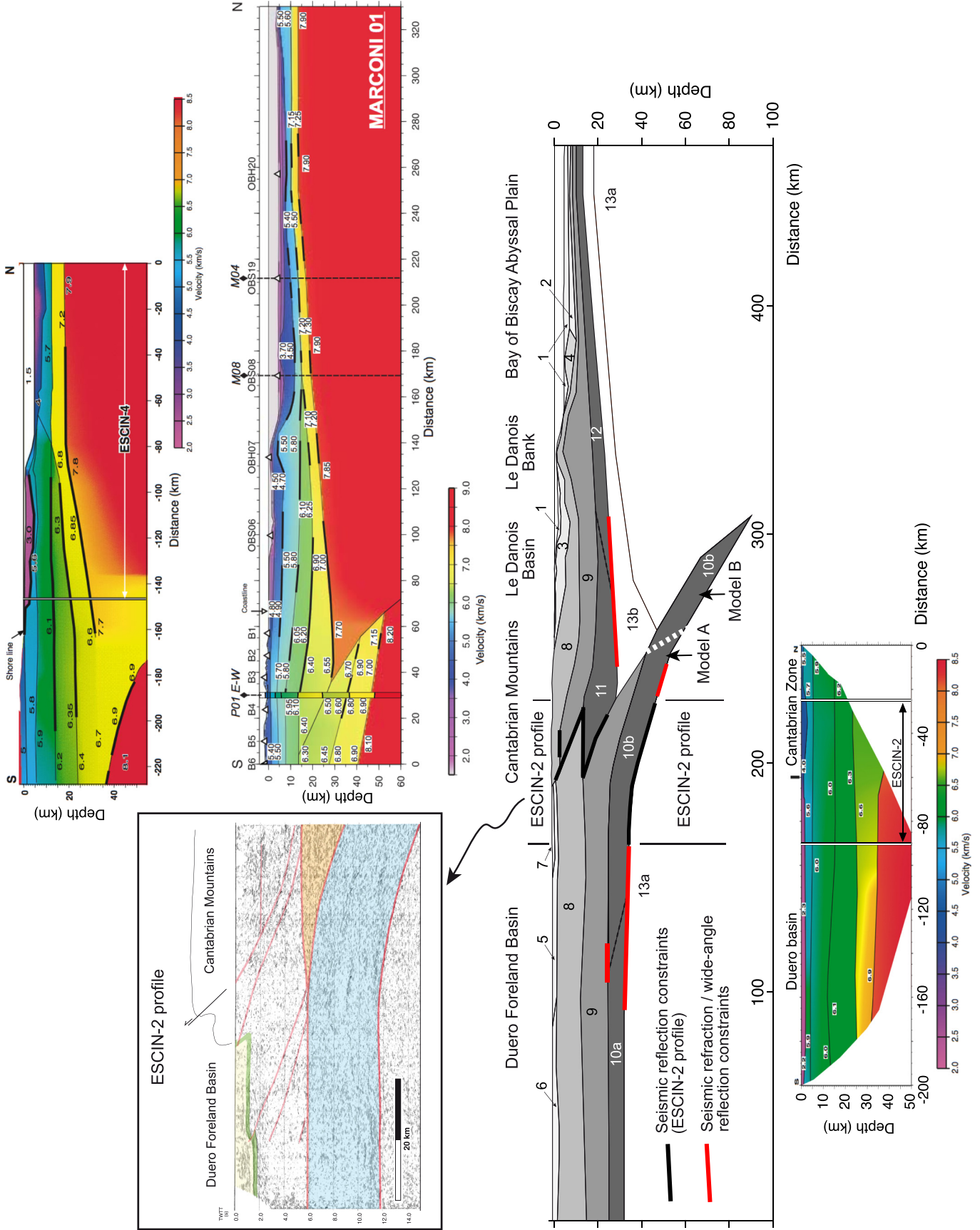


Fig. 2. Detailed geological map of the studied transect, modified from previous synthesis by Alonso et al. (1996), Gallastegui et al. (2002), Quintana (2012) and Rodríguez Fernández et al. (2004). Cities: BU, Burgos; LE, León; OV, Oviedo; SA, Santander; ZA, Zamora. Geological features: CFT, Cantabrian Frontal Thrust; LF, León Fault; LLF, Llanera Fault; MOT, Montes Obarenes Thrust; OB, Oviedo Basin; SCS, Spanish Central System.

Alonso et al. (1996) interpreted the overall structure of the central Cantabrian Mountains as a regional uplift of the Paleozoic basement over a long, north-dipping thrust ramp (the frontal structure of the cordillera) connected to a flat midcrustal detachment. The calculated displacement along this thrust (~25 km) was partially accommodated in a fault-propagation fold developed in the upper part of the crustal ramp. This structure is clearly imaged by commercial seismic lines across the mountain front, as well as in the ESCIN-2 deep seismic reflection profile, where the calculated dip is around 35° (Gallastegui, 2000; Pulgar et al., 1996, 1997). To the south of the frontal thrust, the age of the syntectonic sediments in the Duero foreland basin is poorly constrained due to their coarse-grained continental nature, but recent thermochronometry studies have revealed that the main exhumation phase was Eocene–Oligocene in age and compatible with this structural

model (Fillon, 2012). Although the frontal structure concentrates most of the Alpine deformation, the Leon and Llanera faults (Fig. 2) also reveal significant displacements (Alonso et al., 1996). In the footwall of the latter, the Oviedo Tertiary basin yielded Bartonian–Priabonian flora and fauna near its base (Casanovas-Cladellas et al., 1991).

To the north of the coastline, inverted Mesozoic normal faults and north-verging Alpine thrusts are found in the northern part of the continental platform, the continental slope and the southern border of the abyssal plain. Tertiary succession in the Le Danois basin is mainly marine, with ages ranging from the Upper Paleocene to the Lower Miocene and a total maximum thickness of around 2000 m (Gallastegui, 2000). Further north, thrust sheets stacked in the southern border of the abyssal plain forming accretionary prism-like structures (Fernández-Viejo et al., 2012; Le Pichon et al., 1971). North of Galicia, the first syn-tectonic



Cenozoic sediments of the accretionary wedge are probably Lutetian in age, with post-tectonic sediments on top dated as Burdigalian (Alvarez-Marrón et al., 1997).

3. Geophysical constraints on the crustal structure

In order to constrain the density structure of the whole lithosphere by means of gravity potential field methods, it is important first to define the density structure of the crust as precisely as possible. In this section we will briefly describe some of the key geophysical observations that constrain the crustal model, which are summarized in Fig. 3 and described in more detail in the Supplementary material (text file and Supplementary Fig. 1). The crustal model is a slight modification of the one proposed by Gallastegui (2000), with additional information from the MARCONI-1 seismic refraction and wide-angle reflection data (Ruiz et al., in preparation, modified from Ruiz, 2007).

The ESCIN-2 seismic reflection profile across the central Cantabrian Mountains and northern Duero basin provides a clear image of the whole crust (Pulgar et al., 1996, 1997). The Moho is located at 34 km depth beneath the Duero basin (Gallastegui, 2000) and dips to the north beneath the Cantabrian Mountains, where a complex imbrication is observed between the “Iberian” and “Cantabrian” crusts (Pulgar et al., 1997) (Fig. 3). The Moho is identified down to at least ~53 km depth some 15–20 km south of the coastline, according to wide-angle seismic recordings in on-land stations during the acquisition of the off-shore ESCIN-4 profile (Supplementary Fig. 1a; location of stations in Fig. 2) (Fernández-Viejo et al., 1998; Gallart et al., 1997; Pulgar et al., 1996). The northernmost stations, close to the coastline, did not record the reflection in the north-dipping Iberian Moho; instead, they recorded a shallower, strong phase, interpreted to be the Moho reflection in the Cantabrian margin (Supplementary Fig. 1a). Ray-tracing modeling identifies the “Cantabrian Moho” as south as 10–15 km inland. It is located at 30 km depth beneath the coastline and shallows to ~16–18 km beneath the Bay of Biscay abyssal plain. Wide-angle recordings of the off-shore MARCONI-1 seismic profile, located approximately along the studied transect (Fig. 2), also provided similar results (Ruiz, 2007; Ruiz et al., in preparation). Therefore, both the seismic reflection profile and the wide-angle records are consistent in revealing the north-dipping attitude of the Iberian Moho, subducting beneath the margin in the same way as in the Pyrenees, down to at least 50–55 km. Note that the limited length of the ESCIN-4 profile does not allow recording PmP reflections in the Iberian crust deeper than these values (Supplementary Fig. 1a). The MARCONI-1 profile is longer, but the airguns released less than half the energy used in the ESCIN-4 (Alvarez-Marrón et al., 1996; Ruiz, 2007). If this root is even deeper, as proposed by Gallastegui (2000), it would be difficult to identify due to the poor velocity contrast between eclogitized crustal rocks and mantle peridotites, and the attenuation of the seismic energy along these long-distance paths.

Hence, since the dimensions of the root are not well-constrained, we will test the feasibility of two different geometries: Model A, with a crustal root down to 60 km depth following the seismic constraints (and implying a new balancing of the section, discussed in Section 6.6), and Model B, in which the lower crustal subduction reaches ~90 km depth, as in the reconstruction proposed by Gallastegui (2000).

The crustal basement beneath the Bay of Biscay is known to have been partially consumed beneath North Iberia, creating an asymmetry in the distribution of the sea-floor magnetic anomalies and an accretionary wedge at the foot of the slope (eg. Sibuet et al., 2004; Vissers and Meijer, 2012). However, no evidence of subduction to the south is observed in the wide-angle records (Fig. 3 and Supplementary Fig. 1). Instead, these data point to the underthrusting of this basement and its indentation within the Iberian crust to the south, a process that can explain the same morphological features (Fernández-Viejo et al., 2012; Gallastegui et al., 2002).

The ESCIN-4 wide-angle seismic experiment also revealed that the lower crustal layer along the margin has a rather constant thickness of ~6–8 km and velocities of ~6.6 km s⁻¹ beneath the coastline, increasing up to ~7.2–7.3 km s⁻¹ to the north of the continental slope. This feature was later confirmed by the MARCONI-1 wide-angle seismic experiment, although with a thickness diminished to less than 5 km in most of the marine area (Fig. 3). The nature of this high velocity lower crust (HVLC) will be discussed in Section 6.5. In any case, we must note that its base is a relatively sharp boundary (at least locally) creating PmP-like reflections (Supplementary Fig. 1b), beneath which relatively low P-wave velocities (7.7–7.9 km s⁻¹) suggest partial hydration of the uppermost mantle (Supplementary Fig. 1c). These low velocities are observed as far as the northern end of profile MARCONI-1, close to the foot of the slope of the conjugate Armorican margin (Fig. 3 and Supplementary Fig. 1c).

4. Lithospheric modeling

4.1. Method

The method and associated code (LitMod) used in this paper have been described in detail elsewhere (Afonso et al., 2008). Here we only give a brief overview of some key aspects relevant to our study.

The approach followed is based on the joint 2D modeling of several geophysical observables (gravity anomalies, geoid height, surface elevation and surface heat flow) and seismic proxies (seismic velocities from wide-angle modeling and tomography results) that are interrelated through their dependence on the thermo-physical properties of the crust and mantle.

The temperature within the lithosphere is calculated by solving the 2D steady-state conductive heat transfer equation subject to the following boundary conditions: 1) fixed temperature at the surface of the model ($T_s = 15\text{ }^\circ\text{C}$), 2) no heat flow through the lateral boundaries of the model, and 3) fixed temperature at the lithosphere-asthenosphere boundary (1320 °C). The first-order temperature distribution in the sublithospheric mantle down to 400 km depth is computed assuming adiabaticity (Afonso et al., 2008). To avoid unrealistic sharp discontinuities in the thermal gradient at the base of the lithosphere, a temperature “buffer” is applied between the lithospheric (conductive-dominated) and sublithospheric (convective-dominated) domains, forcing a linear variation of temperature between them. Here we assume a thickness of 40 km for this buffer layer, consistent with results from numerical simulations of mantle-like fluids (e.g. Zaranek and Parmentier, 2004; Zlotnik et al., 2008). Thermal conductivity is constant for each crustal body and dependent on pressure and temperature in

Fig. 3. Seismic constraints used to delineate the crustal structure of the lithospheric model. Top right panels: P-wave velocity models for the ESCIN-4 and MARCONI-1 profiles (location in Fig. 1), from Fernández-Viejo et al. (1998) and Ruiz et al. (in preparation, modified from Ruiz, 2007), respectively. Note the thin crust beneath the abyssal plain, with velocities of ~7.2 km s⁻¹ in the lower crust (HVLC), and the velocities of 7.8–7.9 km s⁻¹ in the uppermost mantle, decreasing to ~7.7 km s⁻¹ in the mantle wedge above the north-Iberian crustal root (see text and Supplementary material for details). Superimposed on the MARCONI-1 profile there is a velocity-depth column corresponding to the intersecting E-W Profile 1 of Pedreira et al. (2003, 2007) showing a high-velocity layer at midcrustal depths that can be laterally linked to the HVLC. Upper left panel: interpretation of the ESCIN-2 profile after Pulgar et al. (1996, 1997) and Gallastegui (2000). Yellow and green shading: Tertiary and Mesozoic sediments of the Duero basin; orange and blue shading depict different attitude of reflectors (see section S1 in the Supplementary text file for a description). Middle panel: sketch of the crustal structure of the model with the seismic constraints superimposed: red lines mark clear seismic refraction/wide-angle reflection interfaces; black lines depict the geometrical attitude of main reflectors in the ESCIN-2 profile (upper left panel). Numbers identify each body in Tables 2 and 3. Lower left panel: P-wave velocity model for Profile 5 (location in Fig. 1) from Pulgar et al. (1996), showing the typical Variscan crustal structure beneath the Duero basin, with upper, middle and lower crustal levels and a total thickness of 32–35 km. Note the increasing seismic velocities in the lower crust to the south (see text for details). Permission granted by John Wiley & Sons, Inc. to reproduce the velocity model of the ESCIN-4 profile (Copyright 1998 by the American Geophysical Union).

the lithospheric mantle, according to the formalism of Hofmeister (1999). Radiogenic heat production is considered to be constant within each body.

Density values for all crustal bodies except for the subducting Iberian lower crust are assumed to be constant. Within the Iberian lower crust and the mantle, densities are calculated following a different approach. Each body is characterized by its chemical composition, defined in the system CaO-FeO-MgO-Al₂O₃-SiO₂-Na₂O, including H₂O and K₂O in some cases. Stable mineral assemblages are computed using a Gibbs free-energy minimization algorithm (Connolly, 2005, 2009). The thermodynamic database used here is the one by Holland and Powell (1998) as modified/augmented by Afonso and Zlotnik (2011) to account for pressures up to ~20 GPa. The density of the whole aggregate (the rock) in each node at the prevailing pressure-temperature conditions is determined through the usual rule of mixtures from the properties of the end-member minerals (Afonso et al., 2008).

From the calculated densities, Bouguer gravity anomalies in 2D are calculated using the algorithm for polygonal bodies of Talwani et al. (1959). The calculation of the geoid height is done following the method outlined in Zeyen et al. (2005). Absolute elevation is first computed under the assumption of local isostasy with reference to a mid-ocean ridge column (Afonso et al., 2008). Then, we also account for flexural support following an approach similar to that described in Jiménez-Munt et al. (2010). To compute the elevation for a given lithospheric density structure, we first calculate lateral changes in lithostatic pressure at the assumed compensation level (400 km depth). We do this by vertically integrating the density distribution over each lithospheric column. If this pressure does not vary laterally, then the lithospheric

structure is locally compensated. Similarly, if loads are partially or totally supported by the rigidity of the lithosphere, significant deviations in pressure will exist at the compensation level. We take these pressure deviations as the flexural load acting on a thin plate (Watts, 2001) to compute the vertical deflection needed to regionally compensate the modeled profile. For this we use the open-source, finite-difference code named tAo (García-Castellanos et al., 1997). With this approach, we find the minimum values of the equivalent elastic thickness T_e for which the calculated profile fits the real profile (ie. the minimum amount of flexural rigidity needed to avoid the vertical isostatic adjustment introducing a misfit in topography or gravity anomalies).

Finally, isotropic seismic velocities (V_p and V_s) are retrieved directly from the energy minimization algorithm (Connolly, 2005). Anelastic effects are computed *a posteriori* as in Afonso et al. (2008).

4.2. Gravity, geoid, elevation and surface heat flow datasets

The regional datasets used as observables to which compare the results of our modeling are displayed in Fig. 4. Fig. 4a shows the elevation over the area investigated, extracted from the global database of Smith and Sandwell (1997) in its version 12.1. Absolute elevation ranges from 2648 m at the highest peak of the Cantabrian Mountains to less than -4600 m in the abyssal plain to the north.

Surface heat flow data are superimposed on top of the topographic image. These come from the compilation of Fernández et al. (1998) for land points and from the Global Heat Flow Database of the International Heat Flow Commission (<http://www.heatflow.und.edu>) for offshore measurements.

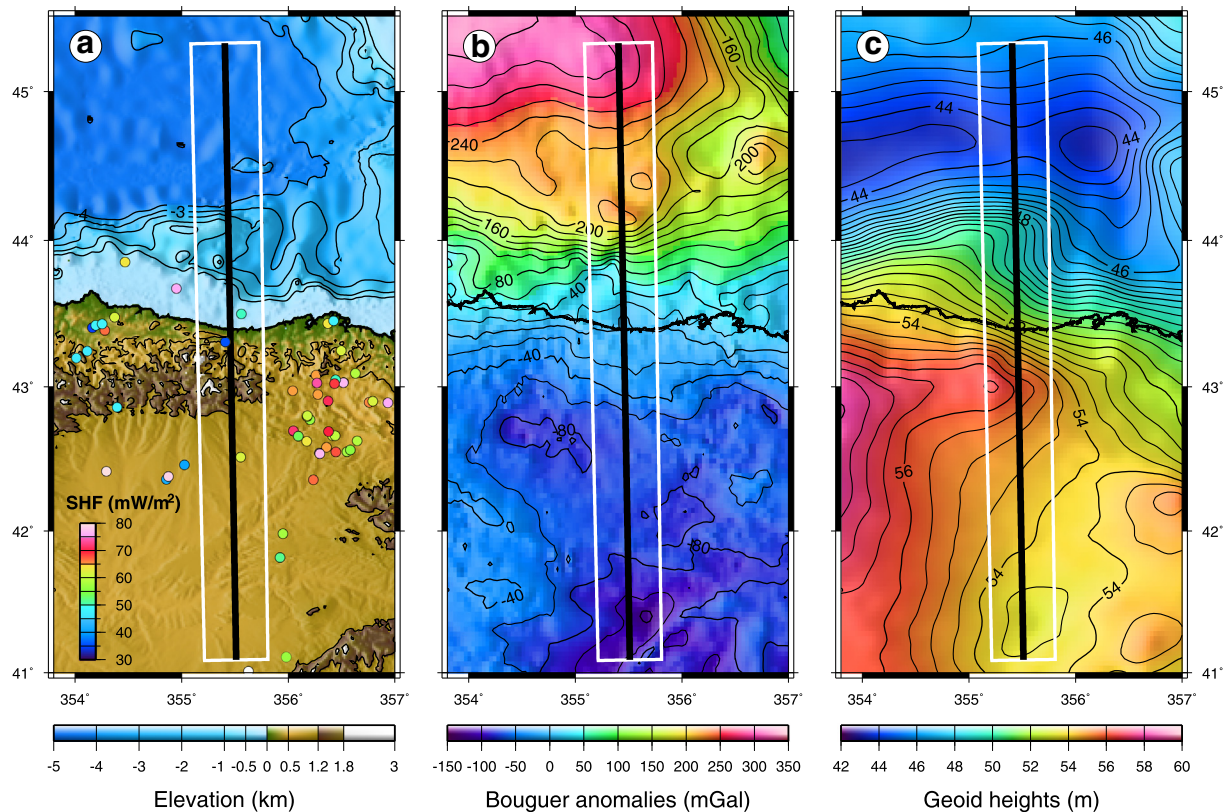


Fig. 4. Maps of regional observables used in this study. a) Elevation (Smith and Sandwell, 1997) with superimposed surface heat flow measurements: onshore data from Fernández et al. (1998) and offshore data from the Global Heat Flow Database of the International Heat Flow Commission (<http://www.heatflow.und.edu>). b) Bouguer gravity anomalies. Land data are taken from a compilation made by Ayala (2013) and marine data were converted from the free air anomaly database of Sandwell and Smith (2009). c) Geoid heights derived from the Earth Geopotential Model EGM2008 developed up to degree 2190 and order 2159 (Pavlis et al., 2012). The thick black line marks the position of the N-S transect modeled in this study. The white rectangle marks the lateral extent of data projected onto the transect to calculate the standard deviations plotted as error bars in Figs. 5 and 7.

On-land gravity data (Fig. 4b) are taken from a recent compilation made by Ayala (2013) in the framework of the Topo-Iberia Project. Off-shore data come from the free air data compilation of Sandwell and Smith (2009) in its version 18.1, and were converted to complete Bouguer anomalies using the FA2BOUG code (Fullea et al., 2008) and a reduction density of 2670 kg m^{-3} . Minimum values below -80 mGal are observed on land in the two main depocenters of the Duero basin, located in its northern and southern borders and created by flexural bending in response to the loads of the Cantabrian Mountains and the Spanish Central System, respectively. Offshore, Bouguer anomaly values increase to the NW as the crust thins in this direction.

Geoid heights (Fig. 4c) were obtained from the Earth Geopotential Model EGM2008, developed up to degree 2190 and order 2159 (Pavlis et al., 2012). We did not remove the low degree and order spherical harmonic terms to eliminate the effects of sources deeper than the maximum depth of the model because these are only expected to create nearly linear trends over this relatively short profile, and these trends are later removed by the code. As expected, higher geoid heights (exceeding 54.5–55 m) are found in the mountainous areas: the Cantabrian Mountains in the central part of the map, the NE tip of the Spanish Central System in the SE corner, the NW tip of the Iberian Range in the eastern border, and the León Mountains immediately to the west of the western edge. Minimum values of less than 44 m are found in the abyssal plain, approximately over the thick syn-tectonic sequence accumulated ahead of the accretionary wedge.

4.3. Density and compositional values

4.3.1. Crust

The densities considered for the different bodies of the model are listed in Table 1. Crustal values were mostly taken from Pedreira et al. (2007). They come from reported density determinations in rock samples or conversions from P-wave velocities (recorded along several seismic refraction/wide angle reflection profiles, as well as in boreholes). A detailed justification for all of them can be found in the aforementioned paper and references therein.

We have included, however, some minor changes detailed in the Supplementary text file (Section S2) and one significant difference referring to the lower crust, which is now split in pieces of different densities. Beneath most of the continental margin, we have increased its density from 2970 kg m^{-3} to 3120 kg m^{-3} to be more consistent with the high seismic velocities ($\sim 7.20 \text{ km s}^{-1}$) found in this zone (Fig. 3). Away from this area of anomalously high velocities, the remaining Cantabrian/European lower crust is assumed to have a density of

2900 kg m^{-3} . This includes the portion that is tectonized and indented into the Iberian crust (with velocities of $6.40\text{--}6.60 \text{ km s}^{-1}$) and the lower crust beneath the Armorican platform.

For the Iberian lower crust, we performed a more detailed analysis of its internal density distribution, since we wanted to test the possibility of subduction down to $\sim 90 \text{ km}$ depth. As mentioned before, we assign a chemical composition and track the density changes induced by mineral transformations, assuming thermodynamic equilibrium. The choice of an appropriate composition/lithology for the Iberian lower crust is therefore an important issue that we address in the following lines.

The southern end of the modeled profile is located close to the first relieves of the Spanish Central System (SCS, Figs. 1 and 2), where xenolith studies reveal one of the most felsic compositions worldwide for the lower crust (Rudnick and Gao, 2003; Villaseca et al., 1999). Alkaline ultrabasic dykes that intruded into the Variscan basement in early Mesozoic times carried a suite of lower-crustal xenoliths composed of felsic granulites ($\sim 95\%$ of the total volume) and much less abundant metapelitic granulites ($\sim 5\%$) and charnokites ($\sim 0.01\%$).

Toward the north, this anomalous felsic end-member gives way progressively to a more mafic composition. Both felsic and mafic granulites equilibrated during the late Variscan orogeny were exhumed by the Mesozoic-Cenozoic tectonic events all along the Pyrenean-Cantabrian belt (Mendia and Ibarguchi, 1991; Vielzeuf, 1984). Similar felsic and mafic granulites were dredged from the seafloor in the northern slope of Le Danois Bank (Fig. 2) as clasts within Early Cretaceous syn-rift conglomerates (Capdevila et al., 1980).

All these observations indicate mafic/felsic compositional layering in the lower crust all along north Iberia. We therefore assume that the composition along the profile studied here changes laterally from “felsic” in the south (although not as felsic as in the SCS) to “intermediate” in the north. For the sake of simplicity, we divided the Iberian lower crust into only two bodies, with a zone of superposition to simulate a gradual change. In absence of further constraints, we placed the limit between them approximately following the strong gradient in seismic velocities observed in the seismic refraction profile 5 (Location in Fig. 1, P-wave velocity model in Fig. 3). Surprisingly, in spite of the more felsic composition, higher seismic velocities in the lower crust are reported near the SCS ($6.8\text{--}6.9 \text{ km s}^{-1}$) than to the north ($\sim 6.6 \text{ km s}^{-1}$) along this profile. This observation can be at least partially explained in terms of water content, if we assume that the lower crust is anhydrous in the south and mildly hydrated to the north. Analysis of S-wave phases along seismic refraction Profile 5 made by Fernández-Viejo (1997) suggest Poisson's ratios <0.25 in the southern part of the profile and >0.25 in the north, an observation that is compatible with

Table 1
Density values and thermal properties used in the modeling.^a

Body # (Fig. 3)	Description	ρ (kg m^{-3})	k ($\text{W m}^{-1} \text{K}^{-1}$)	A ($\mu\text{W m}^{-3}$)
1	Cenozoic in LDB and post-tectonic cover (Mid.-Up. Miocene to recent) in the abyssal plain	2200	2.50	1.20
2	Pre-tectonic and syn-tectonic Mesozoic-Cenozoic sediments in the abyssal plain	2400	2.50	1.20
3	Mesozoic in the continental platform (LDB)	2550	2.50	1.20
4	Accretionary wedge at the foot of the continental slope (mix of sediments and basement rocks)	2550	2.50	1.50
5	Sediments of DB (Mesozoic and mostly Tertiary)	2460	2.53	1.20
6	Sediments of DB (fine-grained, southern part)	2300	2.53	1.20
7	Sediments of DB (conglomerates northern border)	2600	2.53	1.20
8	Upper Crust (pre-Mesozoic basement)	2720	2.40	1.65
9	Middle Crust	2860	2.10	1.00
10a	Iberian Lower Crust (“felsic”, southern part)	b	2.00	0.40
10b	Iberian Lower Crust (“intermediate”, northern part)	b	2.00	0.33
11	European (Cantabrian) Lower Crust, except HVLC	2900	2.00	0.33
12	High Velocity Lower Crust in the continental margin	3120	2.00	0.15
13	Mantle	b	c	0.02

^a Abbreviations are as follows: ρ , density; k , thermal conductivity; A , radiogenic heat production per unit volume; b, density values are dependent on the chemical composition and pressure-temperature conditions (see text and Table 2); c, variable thermal conductivity (pressure and temperature dependent) according to the model of Hofmeister (1999); DB, Duero basin; HVLC, High Velocity Lower Crust; LDB, Le Danois basin.

either more mafic composition and/or higher water content to the north.

Therefore, for the “felsic” part we consider an anhydrous mixture dominated in a 70 wt. % by the composition of the felsic granulite xenoliths from the SCS, with a 30 wt. % contribution from the average global lower crustal composition proposed by Rudnick and Gao (2003), which is dominated by mafic granulites. For the “intermediate” composition, we consider a 50–50% mix between these two end-members, with the addition of 2 wt. % of water. Forward tests have shown that this water content is enough to fit the seismic velocities, and quantities in this order are generally accepted for the lower crust (Hyndman and Shearer, 1989; Semprich et al., 2010). Details on the proportions of the main constituent oxides for both compositions can be found in Table 2. The resulting density values for these particular lower crustal compositions, as well as for the mantle compositions described below, are part of the model results and will be described in Section 5.

4.3.2. Mantle

The composition of the lithospheric mantle is more difficult to determine. To avoid introducing excessive complexity that is not well constrained, and taking into account that no oceanic lithosphere is expected in this part of the Bay of Biscay, we have assumed just one compositional body all along the transect: the average composition for “tecton” (tectonothermal age of the overlying crust < 1 Ga) garnet subcontinental lithospheric mantle (type Tc_1 of Griffin et al. (2009), Table 2). The effects of alternative compositions will be discussed in Section 6.3.

In any case, all tested dry compositions predict P-wave velocities in the range of 8.1–8.2 km s⁻¹ for the uppermost mantle beneath the North-Iberian margin, while seismic studies reported velocities as low as 7.7–7.9 km s⁻¹ (Fig. 3). The easiest way to explain these low velocities is to assume some degree of hydration. The presence of water allows the stabilization of hydrous phases (e.g. serpentines, amphiboles) at temperatures < ~500 °C, causing the decrease in P-wave velocities and densities. Empirical models indicate that velocities of 7.6–7.9 km s⁻¹ in the upper mantle would correspond to H₂O contents of ~1–2 wt. % (Carlson, 2003). Hydration of the uppermost mantle in continental margins tends to vanish with depth, creating rather complex and diffuse

Table 2
Chemical compositions used for the Iberian lower crust and the mantle.

Body # (Fig. 3) →	Iberian lower crust		Mantle		
	“felsic” (south) ^a	“intermediate” (north) ^b	Lithospheric (dry) ^c	Lithospheric (hydrated) ^d	Sublithospheric ^e
	10a	10b	13a	13b	-
SiO ₂	59.91	56.89	44.76	44.31	45.36
Al ₂ O ₃	17.25	16.81	3.52	3.48	4.49
FeO	7.83	7.88	8.05	7.96	8.11
MgO	4.64	5.28	40.04	39.63	38.10
CaO	3.98	5.47	3.12	3.09	3.58
Na ₂ O	2.60	2.56	0.24	0.24	0.36
K ₂ O	2.57	1.97	0.00	0.03	0.00
H ₂ O	0.00	2.00	0.00	1.00	0.00

(Compositions in wt.%. Original percentages recast to 100%).

^a Based on a mixture between the composition of the felsic granulite xenoliths from the Spanish Central System (Villaseca et al., 1999) (70 wt. %) and the average global lower crustal composition proposed by Rudnick and Gao (2003) (30 wt. %).

^b Based on an evenly mixture between the composition of the felsic granulite xenoliths from the Spanish Central System (Villaseca et al., 1999) and the average global lower crustal composition proposed by Rudnick and Gao (2003), plus 2 wt. % of water.

^c Average Tecton Garnet Subcontinental Lithospheric Mantle (Tc_1) (Griffin et al., 2009).

^d Same as above, but with addition of 1 wt. % of water.

^e Primitive Upper Mantle (McDonough and Sun, 1995).

Table 3
Additional compositions tested for the lithospheric mantle.

	Pr_6 Griffin et al. (2009)	PUM-J79 Jagoutz et al. (1979)
SiO ₂	45.4	45.2
Al ₂ O ₃	3.7	4.0
FeO	8.3	7.8
MgO	39.9	38.3
CaO	3.2	3.5
Na ₂ O	0.26	0.33

(Compositions in wt.%. Original percentages recast to 100%).

zones. To keep the model as simple as possible, we have introduced a single body of hydrated mantle with a simple geometry (thickness of 5 km along most of the margin) and constant water content (1 wt. %) added to the Tc_1 lithospheric composition (Table 2).

Finally, the sublithospheric mantle is modeled with a major-element composition representative of the Primitive Upper Mantle, according to McDonough and Sun (1995) (Table 2). To avoid abrupt and unrealistic discontinuities at the LAB, we have added a compositional “buffer” at the base of the lithosphere with a thickness of ~30 km and an intermediate composition between the “tecton” garnet subcontinental lithospheric mantle and the Primitive Upper Mantle previously described.

4.4. Thermal properties

Table 1 lists the thermal conductivity and radiogenic heat production values used in this study. They were chosen according to different sources of information that are briefly described below. A detailed justification of all the values adopted can be found in the Supplementary text file (section S3).

Some of the thermal conductivity data come from measurements in wells, summarized by Fernández et al. (1998). For deeper parts of the crust, conductivity values are assigned based on their composition, temperature and pressure, following experimental work (Clauser and Huenges, 1995; Vosteen and Schellschmidt, 2003). Within the mantle, as mentioned in Section 4.1, we model the effects of pressure and temperature on the bulk thermal conductivity according to the formalism in Hofmeister (1999).

Radiogenic heat production is assumed to be constant within each body of the model (Table 1). Crustal values come from thermal modeling studies (Brunet, 1994), measurements in samples from the area (Fernández et al., 1998; Jiménez-Díaz et al., 2012) and average values according to lithological types (Rudnick and Gao, 2003; Vilà et al., 2010). The mantle is assumed to have a heat production of only 0.02 μW/m³ (Chapman, 1986).

Considering the thicknesses of the crustal layers in the less disturbed part of the model beneath the Duero basin (2500 m for sediments and 13, 10 and 8 km for the crystalline upper, middle and lower crusts, respectively), the weighted average heat production in the whole crust is 1.11–1.12 μW/m³, which fits well with the standard continental crust heat production of 1.03 ± [0.74 – 1.38] μW/m³ proposed by Vilà et al. (2010), and lies also between the averages for Paleozoic orogens (0.96 μW/m³) and Mesozoic–Cenozoic contractional orogens (1.17 μW/m³) according to Rudnick and Fountain (1995).

5. Results

5.1. Model A: shallow crustal root (~60 km depth)

Fig. 5 shows the observed and calculated values of surface heat flow, Bouguer anomaly, geoid undulation and elevation for Model A (“shallow” crustal root), according to the constraints and assumptions described in the previous sections. We accounted for the decrease in

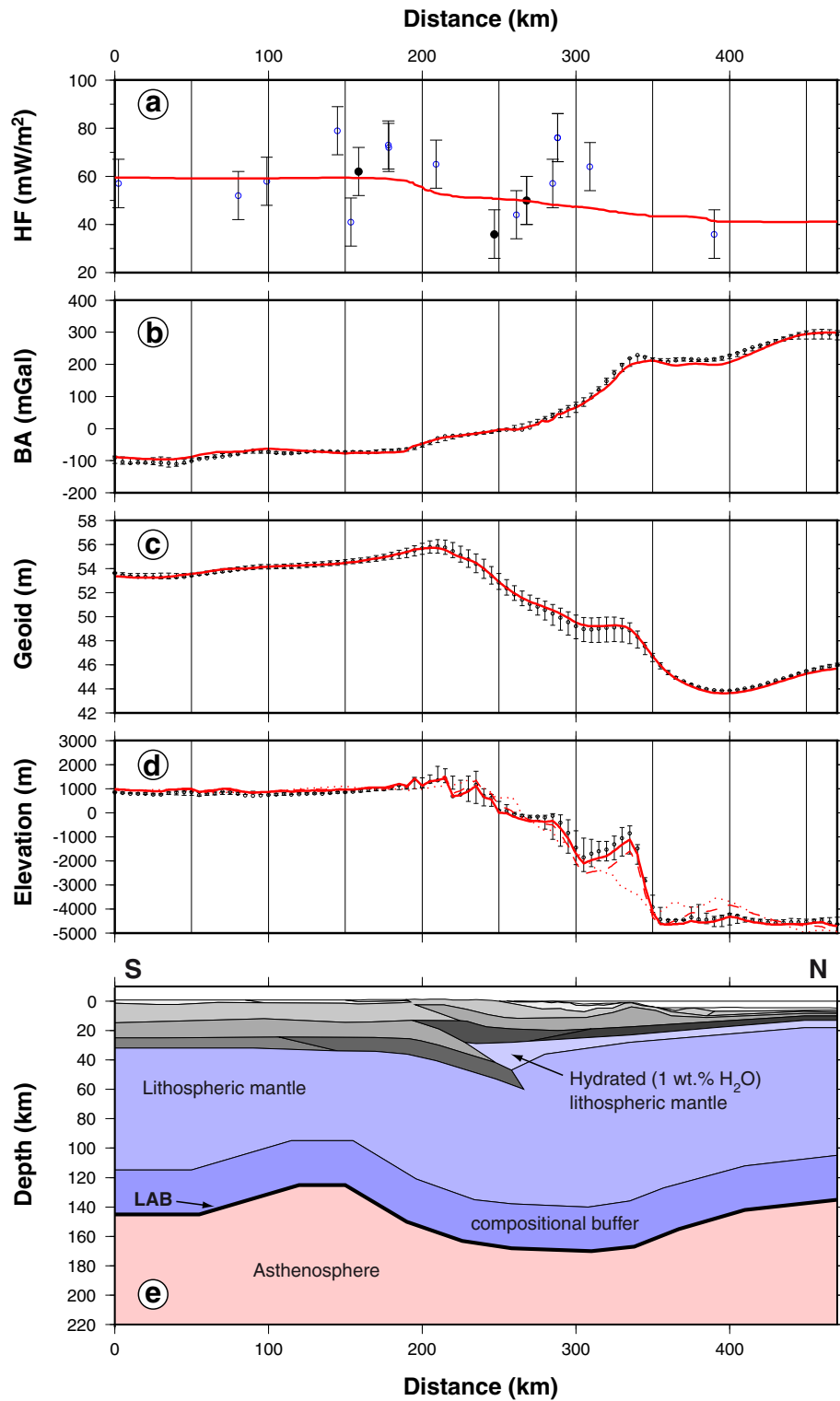


Fig. 5. Modeling results for Model A, showing the fitting of surface heat flow (HF), Bouguer anomaly (BA), Geoid and Elevation. Except for heat flow values, black dots mark the observed values along the transect, and error bars represent ± 1 standard deviation according to values observed 25 km to the east and to the west of the transect (white rectangles in Fig. 4). Heat flow values are orthogonally projected onto the section from lateral distances ≤ 10 km (black dots) or ≤ 50 km for land data and ≤ 100 km for marine data (blue dots). Red lines indicate the calculated responses of the model (with a Gaussian filter for the case of the surface heat flow to avoid short-wavelength spikes). In the elevation plot, red dotted and dashed lines represent calculated elevation in the case of effective elastic thickness $T_e = 0$ km (Airy-type isostatic equilibrium) and $T_e = 10$ km, respectively. The continuous red line represents the calculated elevation for $T_e = 30$ km (see text for details).

the water column thickness and the increase in crustal thickness in the nearby Armorican margin by prolonging the bodies (and adjusting the curves) 300 km beyond the limits of the figure to the north (see

Supplementary Fig. 2). Calculated temperatures, densities and P-wave velocities down to 225 km depth are shown in Fig. 6. The density structure of the crust and uppermost mantle is constrained by the Bouguer

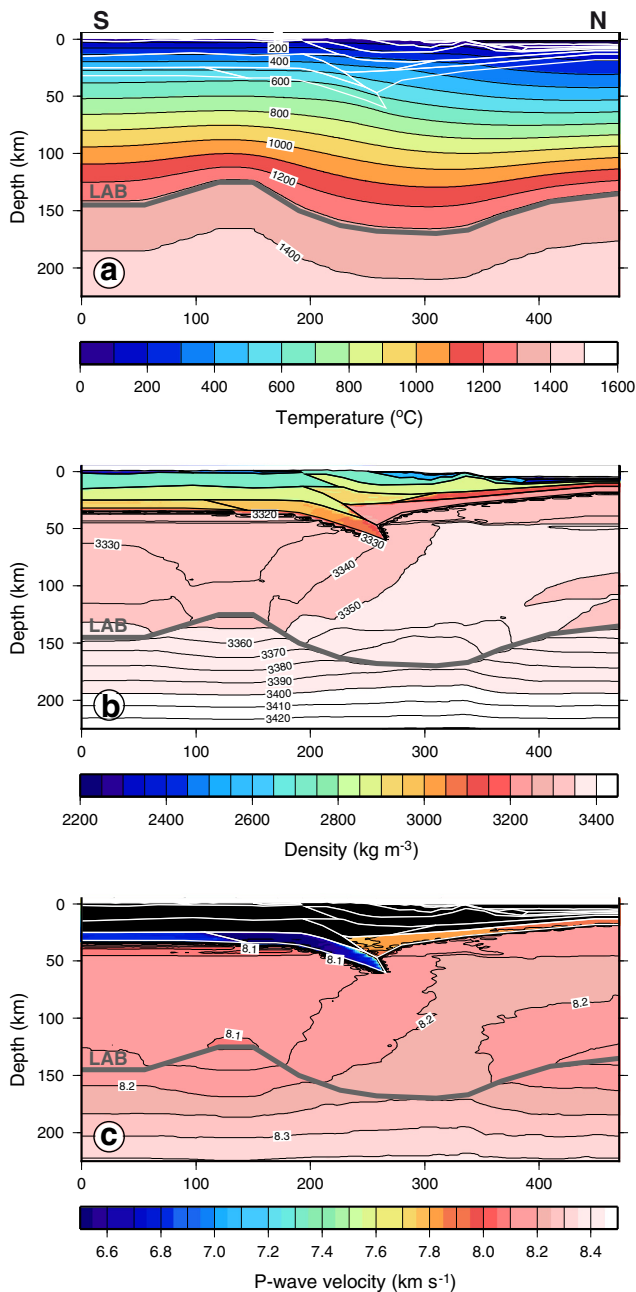


Fig. 6. Thermal, density and P-wave velocity structure along the modeled transect for Model A. The grey bold line (LAB) represents the base of the thermal lithosphere.

anomaly and the short-wavelength component of the geoid undulations, whereas the lithospheric thickness is mainly constrained by the elevation, the long-wavelength component of the geoid and, to a lesser extent (due to the long dispersion bars) by the surface heat flow. As observed in Fig. 5, the calculated response of the proposed lithospheric model fits satisfactorily the regional trends of all these observables.

Elevations are correctly reproduced throughout the model only when some degree of flexural support is considered (continuous line in Fig. 5d). Theoretical elevations according to local (Airy) type of isostatic equilibrium are represented in Fig. 5d by a dotted line. Areas where the absence of local isostatic equilibrium is most evident include the Le Danois bank (at $x = 300\text{--}350$ km), the southern border of the abyssal plain ($x = 350\text{--}425$ km) and the zone immediately above the

deepest part of the crustal root ($x = 250\text{--}265$ km). Forward modeling indicated that an effective elastic thickness of ~ 30 km is enough to reproduce the observed elevations. This is a reasonable value for Variscan and Alpine lithospheres according to results based on “Bouguer coherence” and “free-air admittance” methods (Pérez-Gussinyé and Watts, 2005).

Outside the crustal root, the density of the Iberian lower crust increases toward the north as the composition becomes more mafic. The average density for the southern part of the Iberian lower crust (with the “felsic” composition, Table 2) is 2941 kg m^{-3} , while beneath the northern part of the Duero basin (where the lower crust has the “intermediate” composition) it increases up to 2987 kg m^{-3} . P-wave velocities, on the contrary, decrease toward the north as the water content increases, from an average value of 6.81 km s^{-1} in the region with the felsic composition, to 6.52 km s^{-1} beneath the northern border of the Duero basin (intermediate composition with 2 wt. % of water). These results are in close agreement with the velocity values observed along the seismic refraction/wide-angle reflection profile 5 (Fig. 3). In the crustal root, eclogitization/reactions start at $\sim 40\text{--}45$ km depth, but densification is limited due to the presence of felsic constituents and hydrated phases such as phengite. Maximum densities and P-wave velocities are 3110 kg m^{-3} and 6.83 km s^{-1} , respectively.

Calculated seismic velocities in the hydrated uppermost mantle lie in the range $7.79\text{--}7.88 \text{ km s}^{-1}$. These velocities match perfectly with the values observed below the Bay of Biscay along the ESCIN-4 and MARCONI-1 profiles, except for the southernmost edge of the mantle wedge on top of the subducting Iberian crust, where observed velocities are $\sim 7.7 \text{ km s}^{-1}$ (Fig. 3). Forward tests have indicated that in this small area, a water content of 2 wt. % is necessary to fit the observed velocities. The average density for the hydrated mantle layer is 3236 kg m^{-3} . Temperature is low enough to allow serpentinization reactions ($T < 550$ °C, Fig. 6a), but the small quantities of water available are consumed in this case by other hydrated phases such as clinoamphibole, chlorite, phlogopite and talc. According to Früh-Green et al. (2004), early phases of hydration are commonly marked by the alteration of primary orthopyroxene to form talc- and/or amphibole-bearing \pm chlorite assemblages, like the ones predicted in our model.

The lithosphere-asthenosphere boundary was introduced in the model with the simplest geometry that is able to achieve a reasonable fit of the observables. Lithospheric thickness varies in a significant way across the model: 145 km beneath the southern part of Duero basin, 125 km beneath the northern part of the basin, 170 km under the crustal root, and 160–135 km (shallowing toward the north) beneath the floor of the Bay of Biscay abyssal plain.

The density structure of the mantle is shown in Fig. 6b. Within the lithosphere, the increase of density with depth by the effect of pressure generally dominates over the density decrease by thermal expansivity. However, since the base of the lithosphere is isothermal, thinner lithospheric columns are globally warmer, less dense and less sensitive to the effect of pressure than thicker ones. Density values vary between 3309 kg m^{-3} just beneath the Iberian Moho to 3380 kg m^{-3} in the deepest part of the lithospheric root, within the compositional buffer. A density jump observed at ~ 45 km depth, more pronounced in the northern part of the section, corresponds to the phase change between spinel-peridotites and garnet-peridotites. In the convective part of the mantle beneath the LAB, where the increase in temperature with depth is reduced to the adiabatic gradient, the stronger effect of pressure induces a steeper increment of density with depth.

5.2. Model B: deep crustal root (~ 90 km depth)

At a crustal scale, Model B is the same as Model A except for the larger thickness of the Iberian crustal root, which in Model B reaches 90 km depth, to test the feasibility of the reconstruction proposed by Gallastegui (2000). This change introduces some variations in the

long-wavelength components of the calculated curves of Bouguer anomaly, geoid, elevation and surface heat flow, which we corrected by changing the topography of the LAB.

Fig. 7 shows the fitting of observables, and Fig. 8 displays the calculated temperature, density and P-wave velocity values down to 225 km

depth. In the crustal root, densities and velocities increase up to 3185 kg m^{-3} and 7.07 km s^{-1} , respectively. These are still lower than usual averaged determinations in eclogites at those depths (eg. Christensen and Mooney, 1995), but they are explained again by the presence of felsic components and hydrated phases such as phengite,

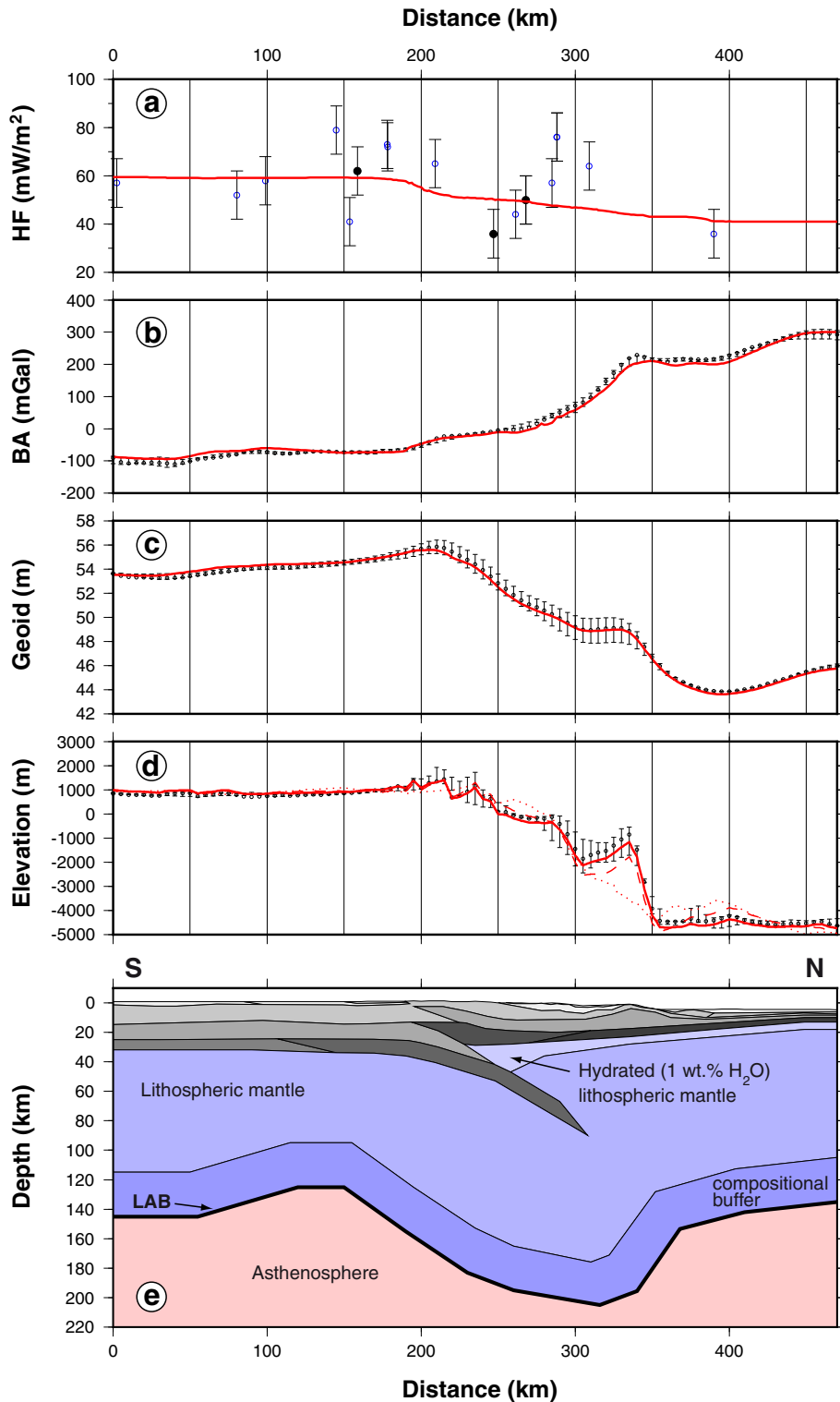


Fig. 7. Same as Fig. 5 but showing results for Model B.

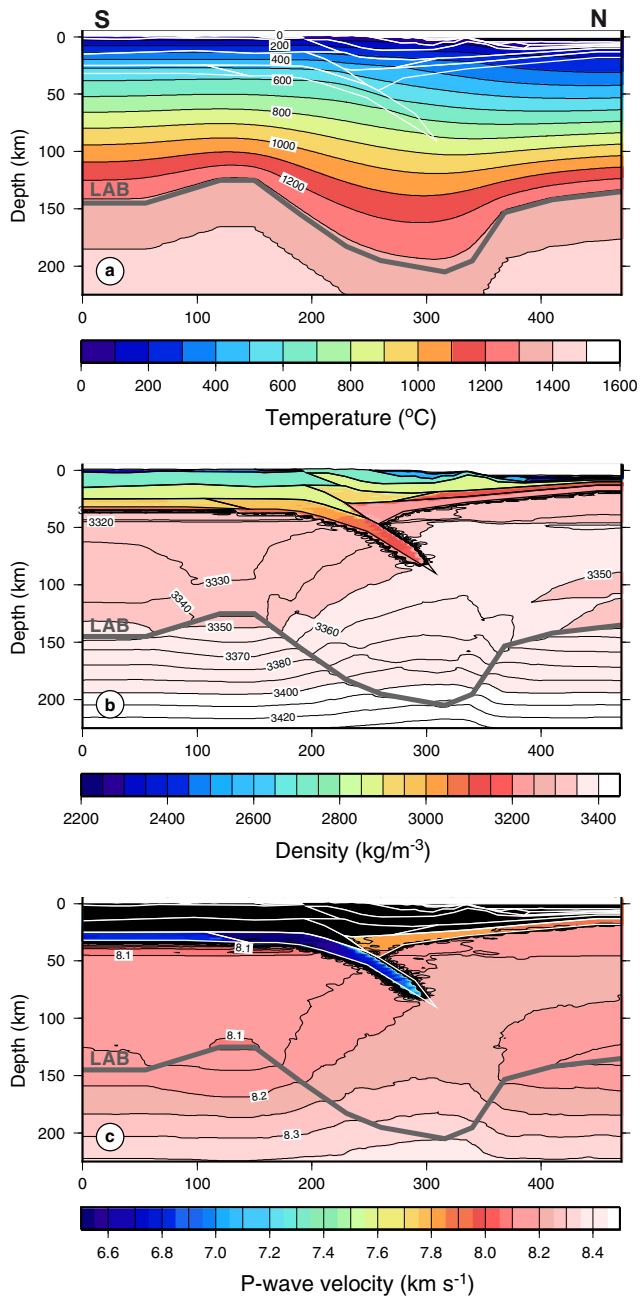


Fig. 8. Same as Fig. 6 but showing results for Model B.

whose stability field is large enough to allow its presence at 90 km depth. The mass deficit created by the root with regard to Model A is compensated here by increasing the thickness of the lithosphere up to 205 km beneath the crustal root. This makes the lithospheric column globally colder and denser. In fact, this is the only change introduced in the LAB with regard to Model A. Note that even in Model B the code predicts a state of near-local-isostatic equilibrium over the deepest part of the crustal root (at $x = 275\text{--}300$ km), whereas deviations supported by flexural rigidity are found both landwards (at $x = 250\text{--}275$ km, related to the buoyancy induced by the higher volume of hydrated mantle on top of a crustal root that is not yet fully densified) and oceanwards (related to the weight of Le Danois Bank resting on top of a flat Moho).

In summary, from the geophysical point of view, both models A and B can explain the observed gravity and geoid anomalies, topographic elevations, and surface heat flow over the area. They are based upon a wide range of seismic information (reflection, refraction and wide angle profiles), although model B considers that the Iberian crustal root extends to a greater depth that is not constrained (although not contradicted) by the seismic information. The main implication in this case is that the lithospheric root must also be deeper than in Model A.

In the next section, we discuss the appropriateness of some assumptions and choice of model parameters, describing their effects on the modeling results and the implications for Model A and B. Finally, we present a tentative evolutionary model that is able to explain the shallower crustal root of Model A, as an alternative to the reconstruction of Gallastegui (2000), valid for Model B.

6. Discussion

6.1. Composition and densification of the subducting Iberian lower crust

Two important assumptions are made when modeling the density structure of the Iberian lower crust and mantle: first, the assumption of thermodynamic equilibrium under thermal steady-state conditions, and second, the specific chemical composition. The steady-state assumption can be considered reasonable in this case, since the last important thermal event (Late Cretaceous volcanism) ended at ~ 85 Ma. After that, the building of the Pyrenean-Cantabrian belt occurred at a low convergence rate (~ 2.5 mm/yr on average) and ended at $\sim 16\text{--}20$ Ma (Alvarez-Marrón et al., 1997; Beaumont et al., 2000; Gallastegui, 2000). Regarding the assumption of thermodynamic equilibrium that is usually valid for the mantle, we emphasize that it may be less reliable under the low temperatures prevailing in the crust, especially under anhydrous conditions. However, since our analysis is restricted to the lower crust, and especially focused in the transformations that occur in the root at depths >40 km and temperatures above ~ 600 °C, we consider that this assumption is reasonable.

Outside the crustal root, the Iberian lower crust with 2 wt. % H_2O in our models would be composed of hydrous greenschist-amphibolite facies assemblages, according to the pressures and temperatures registered (686–988 MPa and 467–579 °C). This contrasts with the granulitic nature of most of the lower crustal sections outcropping along the Pyrenean-Cantabrian belt (Vielzeuf, 1984), although these sections are partially retrograded to amphibolitic paragenesis during their post-variscan history (Mendia and Iburguchi, 1991; Vielzeuf, 1984). We consider it is reasonable to assume that re-equilibration under prevailing conditions in the base of the crust is complete at present, due to the long residence time at relatively high temperatures. In any case, the potential issue of lacking complete equilibrium should not affect our conclusions to a significant extent. If remnants of metastable granulites are preserved in the lower crust, these can be virtually indistinguishable from gravity methods, owing to the fact that densities of granulites and amphibolites can be very similar (Christensen and Mooney, 1995).

There are, however, some implications in the case of generalized granulite preservation, derived from the fact that granulites are nominally anhydrous rocks. If water is absent, reproducing the observed variations in P-wave velocities of the Iberian lower crust along Profile 5 with granulitic compositions would imply a strong increase of mafic components toward the south, contrary to what is suggested by the geological evidence and the decrease in the Poisson's ratio in this direction. Another implication is that densification of the granulitic root by eclogitization processes would be greatly hampered, as these reactions are catalyzed or significantly speeded up by the presence of fluids (Austrheim et al., 1997; Engvik et al., 2001). The final consequence is that this granulitic lower crust, even if it were completely mafic, would be more buoyant in the deepest part of the root than the

amphibolitic (and then eclogitized) lower crust (Christensen and Mooney, 1995).

6.2. Hydration of the upper mantle in the continental margin

One of the questions that arise from the above discussion is the possible relationship between dehydration of the subducting greenschist/amphibolitic Iberian lower crust and the hydration of the upper mantle wedge located immediately on top of it. Released water could potentially rise as vapor phase and be incorporated into the structure of hydrous minerals in a shallower and colder part of the mantle. To evaluate this, we have plotted in Fig. 9a and b the amount of free water (ie. water

that is not incorporated into mineral structures) as a function of pressure and temperature, for the compositions of the subducting lower crust and the hydrated upper mantle, respectively, assuming thermodynamic equilibrium. Superimposed on these graphs, we have marked the range of pressure-temperature conditions that are found inside these bodies in models A and B. As observed, the root in Model A preserves all the water into the structure of hydrous minerals, whereas the root in Model B, begins to dehydrate at $T > 650$ °C, but even in the deepest part of the root, water released is less than 0.8 wt. %. The hydrated mantle body, on the other hand, is always at $T < \sim 550$ °C, and therefore is cold enough to preserve the initially assigned 1 wt % of water within the structure of hydrated minerals (Fig. 9b).

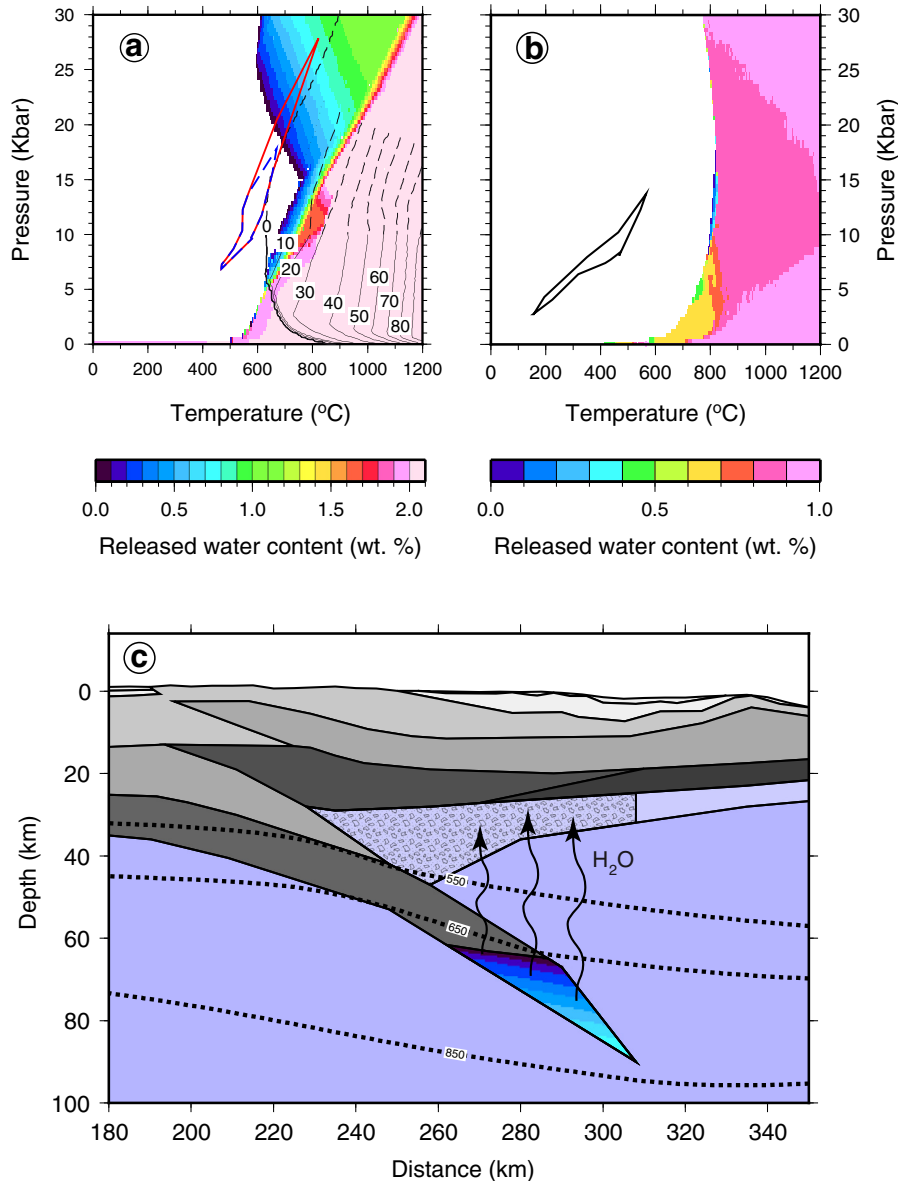


Fig. 9. Schematic illustration of the water balance between the dehydrated subducting lower crust and the overlying hydrated mantle wedge. a) In color scale: released water (in wt. %) of the subducting Iberian lower crust (body 10b, Fig. 3 and Table 2) calculated using *Perple_X* (Connolly, 2005, 2009). In black contours: percentage of partial melt (wt. %) for the same composition, calculated with *Perple_X* using the “melt(HP)” model (Holland and Powell, 2001; White et al., 2001) (note that this model may not be very accurate for pressures > 10 kbar). The superimposed blue and red outlines mark the pressure-temperature conditions for the subducting Iberian lower crust (body 10a), for models A and B, respectively. Note that only the deepest part of the root in Model B releases some water during eclogitization reactions, and that partial melt is not predicted, or it forms in negligible amounts. b) Same type of diagram but for the body of hydrated upper mantle, with 1 wt.% of H₂O in its composition (body 13b, Fig. 3 and Table 2). As observed, this body keeps the 100% of the structural water unless heated up to more than ~ 700 °C. c) Detailed view of the crustal root and the mantle wedge on top of it, with some key isotherms (units in °C) explained in the text. The lower crust begin to dehydrate by eclogitization reactions at temperatures above 650 °C (region coloured with the same scale than in a)), but the released water is only $\sim 12\%$ of the necessary input to hydrate the uppermost mantle on top of it (body in light mauve with texture) with 1 wt. % of water (see text for details).

A very rough balance based on the present-day thermal structure indicates that the released water during eclogitization of the lower crustal root (depicted in Fig. 9c with the same colorbar scale of Fig. 9a) is only about ~12% of the required water to hydrate the mantle wedge on top of the root (dotted area in Fig. 9c). Even if the subducting crust was ~100 °C hotter at the time these processes occurred, it would still be far from extensive dehydration (Fig. 9a). Moreover, the amount of water released can be considered as a minimum estimate because (1) anhydrous granulitic relicts might also be present before the subduction started, and (2) water content in the innermost part of the mantle wedge must be in the order of 2 wt. % to explain seismic velocities as low as 7.7 km s⁻¹ locally observed there in both the ESCIN-4 and MARCONI-1 profiles (Fig. 3). Therefore, other sources of water supply must be involved.

The effect of partial melting in the subducted lower crust represents another possible source of water, as these melts can potentially rise into the mantle wedge, becoming water-saturated as they decompress, and expelling free water. We have computed the amount of partial melt expected for the composition of the lower crust according to the melt model of Holland and Powell (2001) and White et al. (2001). As observed in Fig. 9a, partial melt is not expected, or it may occur in negligible amounts, for the pressure-temperature conditions inside the crustal root. If any melt was formed, it would be far from the critical percentage necessary to migrate and rise, considering that fractions of ~7% mark the threshold for melt connectivity along grain boundaries (Rosenberg and Handy, 2005). Therefore, partial melting of the subducting lower crust can be ruled out in this case as a major supplier of water into the mantle.

On the other hand, apart from the mantle wedge located immediately on top of the subducting Iberian crust, mild hydration of the uppermost mantle seems to be also necessary all along the Bay of Biscay in order to explain the relatively low P-wave velocities of 7.8–7.9 km s⁻¹ observed beneath the HVLC. From the above analysis we conclude that the hydration of the upper mantle must be essentially related to infiltration of water from the seafloor during the Mesozoic rifting episode that led to the formation of the Bay of Biscay.

6.3. Composition and thickness of the lithospheric mantle

Both models A and B presented in this paper indicate that a relatively thick lithospheric mantle (even far from the orogenic region) is necessary to simultaneously fit all the observables. The modeled thickness of the lithospheric mantle is influenced by its thermal structure and composition, as well as by the density and thickness of the overlying crust. The thickness of the crust is well constrained due to the numerous deep seismic lines available in the area. Obtaining densities from P-wave velocities allows some range of variations, and increasing the density of the crust would allow considering a lighter mantle, which can be attained by raising the LAB. However, the density values we used for the crust already are at the upper bound of common P-wave to density conversions (eg. Christensen and Mooney, 1995; Ludwig et al., 1970) and are very similar or even higher than the values used in other gravity models in North-Iberia (Casas et al., 1997; Fernández-Viejo et al., 1998; Gallastegui, 2000; Pedreira et al., 2007; Torne et al., 1989).

Modifying the thermal structure to make an overall colder lithosphere would also allow raising the LAB to counterbalance. In this study, the base of the thermal lithosphere is fixed at the constant temperature of 1320 °C, which is within the limited range of commonly accepted values (eg. Artemieva, 2009), but the temperature at the Moho is less constrained and could potentially be lowered by decreasing the heat productivity in the crust. However, the radiogenic heat production in our model, at least for the felsic nature of the crust in the southern end of the profile, may be already relatively low, and we don't expect

Moho temperatures significantly below the calculated ~550 °C in this part of the profile, where the LAB reaches 145 km depth.

Chemical composition of the mantle is the other source of density variations we can claim. Continental lithospheric mantle is expected to be compositionally heterogeneous due to different ages, melt extraction, refertilization, etc. In the following, we explore the effects of considering more fertile compositions for the lithospheric mantle, implying higher average densities and allowing for a reduction in thickness. For example, Carballo et al. (2015) consider the continental mantle beneath the Pyrenees to be represented by the average composition of lherzolites from the Lherz massif (Pr_6 of Griffin et al. (2009)). This compositional type represents metasomatic refertilization of a refractory harzburgite, with P-wave velocities and densities that are virtually indistinguishable from those of the Primitive Upper Mantle composition of Jagoutz et al. (1979) (PUM-J79). The PUM-J79 type is slightly less enriched than the PUM composition of McDonough and Sun (1995) (PUM-MS95) usually ascribed to the asthenosphere, and has been considered as a reasonable average composition for the continental lithospheric mantle in areas subjected to significant extension and refertilization, close to oceanization (eg. Fulla et al., 2010; Carballo et al., 2015). In Fig. 10 we compare the depth-density profiles calculated at three different locations along Model A (X = 0, 266 and 470 km) for the composition used in this work (Tc_1), and the alternative Pr_6 and PUM-J79 compositions. The results show that density differences are very small all along the three lithospheric columns, in spite of their differences in crustal and lithospheric thickness. Forward-modeling tests have indicated that using the most dense composition allows for a reduction in the lithospheric thickness of no more than ~5 km.

We may conclude that the thickness of the thermal lithosphere as it is defined in this work (ie. the top of the convective-dominated part of the mantle) must be close to the thickness displayed in our models in order to explain all the observables. We must note, however, that the resolution of this modeling strategy depends on a long list of uncertainties derived from the measurement/processing/choice of observables and model parameters that are difficult to assess formally. A full uncertainty analysis of a similar method has been recently performed by Afonso et al. (Afonso et al., 2013a,b), which suggest that estimated LAB depths (strictly, the depth to a geotherm) are typically affected by uncertainties (i.e. one standard deviation) of the order of ± 10–15%.

6.4. P-wave velocities and comparison with seismic tomography results

The only relevant difference in the LAB topography between models A and B is the greater depth inferred in Model B beneath the crustal root, reaching more than 200 km. The calculated P-wave velocity structures for both models (Figs. 6 and 8, lower panels) allow us to test which one is more consistent with published P-wave tomography models. Fig. 11 illustrates this comparison, in which all the sections are expressed in relative perturbations of P-wave velocities with respect to the ak135 reference model (Kennett et al., 1995). Fig. 11a, b and c show the structure of the studied transect from 40 to 400 km depth, according to the tomographic model of Villaseñor et al. (2003), and to our models A and B, respectively. The amplitudes of the P-wave perturbations are somewhat greater in our synthetic sections. This is to be expected, as it is well known that the amplitudes recovered by tomography models based on ray theory are underestimated (Foulger et al., 2013; Hung et al., 2001). We should therefore restrict our comparison to the general distribution and shape of the anomalies, not to their amplitudes. Probably the most conspicuous feature in the tomographic slice is the low velocity anomaly located in the top-central part of the section, extending down to ~90 km depth. This can be correlated with the low-velocity anomaly created in our synthetic models by the crustal root and the hydrated mantle wedge on top of it. This feature seems to be better reproduced in Model B, but the exact geometry of such a

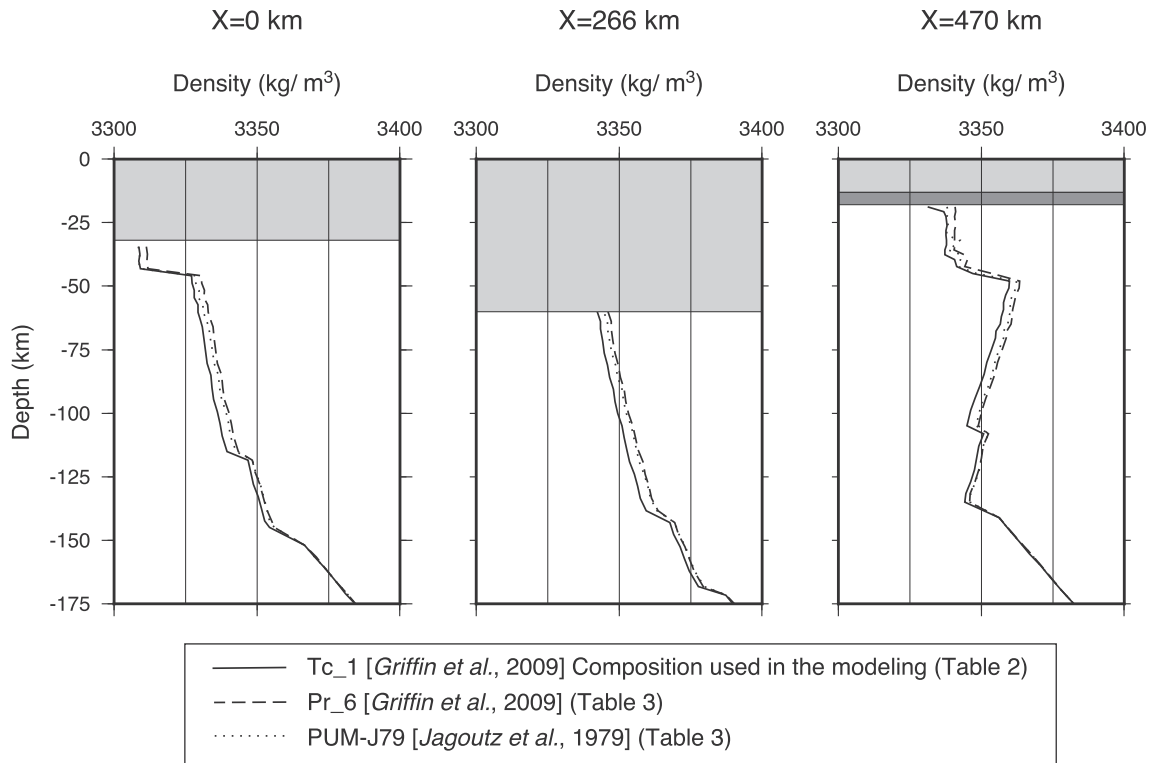


Fig. 10. Depth-density profiles for the lithospheric mantle of Model A at horizontal distances of $X = 0$ km (southern end, undisturbed Variscan crust), $X = 266$ km (deepest part of the Alpine crustal root) and $X = 470$ km (northern end, Bay of Biscay), and for three different compositions: Tc_1, Pr_6 and PUM-J79 (Griffin et al., 2009; Jagoutz et al., 1979) (Tables 2 and 3). In each curve, the composition of the lithospheric buffer is a 50–50% mix between the corresponding lithospheric composition and the sublithospheric PUM-MS95 composition (McDonough and Sun, 1995) (Table 2). Light grey areas represent the depth range occupied by the crust in each profile. The dark grey band in the profile for $X = 470$ km represents the hydrated part of the mantle beneath the Bay of Biscay. Note that very small density variations are observed between these three different mantle compositions along the model. Using the most dense composition (Pr_6) instead of Tc_1 allows for a reduction in the lithospheric thickness of ~5 km.

shallow tomographic anomaly beneath the coastline is not well constrained. In Fig. 11a we can also identify a relatively flat surface at ~220 km depth with anomaly values around zero, separating a lower part with slow anomalies from an upper part with dominantly fast anomalies. This feature is slightly better reproduced in Model A, since the deep lithospheric root in Model B creates a depression in the isonomaly countours.

In spite of the poor resolution in the northern part of the tomographic section due to lack of seismic stations in the Bay of Biscay, the fast anomaly in the lithosphere is satisfactorily reproduced, especially in Model A, where it remains at a shallower position than in Model B. Interestingly, the shape of this anomaly in Fig. 11b and c gives the impression of a southward-directed slab, a finding that could serve as a caution advise when interpreting slow anomalies in tomographic sections. In the southern part of the tomographic profile (Fig. 11a), the upper 200 km of the mantle depict very subtle velocity anomalies, whereas our models show a thick, cold and fast lithosphere, with an uplift of the LAB around model distances of 120–170 km.

The most recent tomographic model of Chevrot et al. (2014) provides additional constraints to check the presence of this particular feature. These authors published a set of horizontal slices of a P-wave tomographic model obtained after the dense deployments of the PYROPE and IBERARRAY seismological stations. Fig. 11d shows the horizontal slice of the area studied here, with anomalies averaged for depths between 125 and 150 km, after crustal correction. On top of this map, we have also plotted the calculated anomalies of our synthetic models for the same depth interval: results for Model A are depicted to the left of the central line marking the studied transect, and results for Model B are represented to the right. Again, the absolute

value of the calculated anomalies do not match the tomographic anomalies, but if we make them only 0.65% slower, as depicted in Fig. 11d, the match is strikingly good. As observed, there is an E-W trending band of relatively slow anomalies between 42 and 43°N that is spatially coincident with the area of uplifted LAB in our model. This elongated slow anomaly extends all along the length of the Pyrenean-Cantabrian belt and its origin remains enigmatic (Chevrot et al., 2014). According to the geometry of the LAB, we suggest it may be related to bending of the weak lower lithosphere (decoupled from the upper lithosphere) or to thermal erosion perhaps by small-scale edge-driven convection at the borders of the lithospheric root (eg. Missenard and Cadoux, 2012). This slow anomaly is flanked to the north by a parallel fast anomaly that Chevrot et al. (2014) attributed to a cooler European lithosphere, and that we explain with the presence of the lithospheric root. As before, the match is slightly better for the case of Model A, since Model B predicts a stronger negative anomaly at 43.5–44°N, related to the more pronounced lithospheric root. However, although we can conclude that our modeling results are broadly compatible with the tomographic studies, more detailed tomographic models are needed before we can strongly favor Model A or Model B.

6.5. The nature of the HVLC

The high-velocity lower crustal body (HVLC) of the North-Iberian margin is one of the most remarkable features in both the ESCIN-4 and the MARCONI-1 wide-angle models (Fig. 3). It seems clear that it does not correspond to purely stretched lower continental crust because its velocities are too high for lower crustal rocks located at such shallow

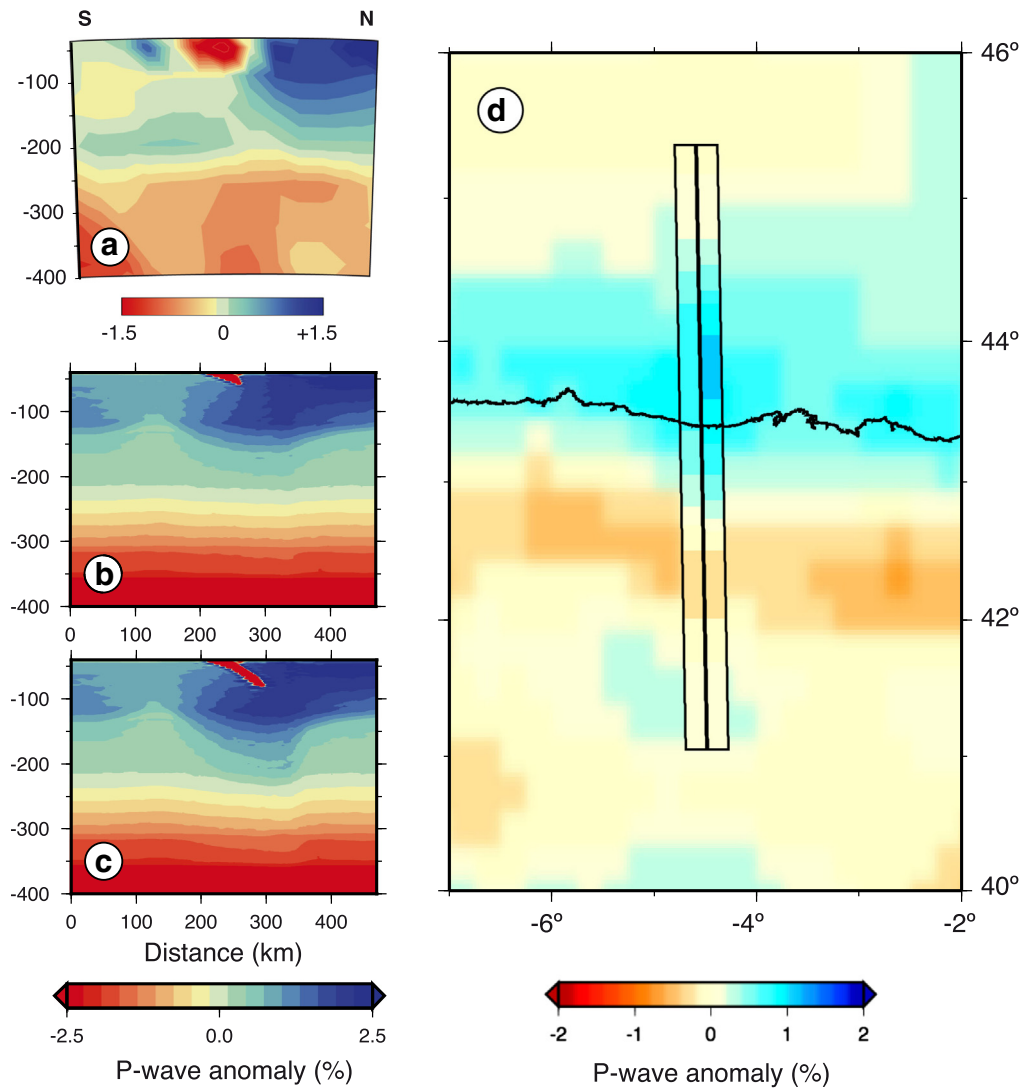


Fig. 11. Comparison between the P-wave velocity structure calculated for the mantle along the transect and the results of tomographic models in the same area. All plots represent percentage of velocity deviations with respect to the ak135 reference model (Kennett et al., 1995). a) vertical slice of the tomographic model of Villaseñor et al. (2003) along the studied transect. b) and c), synthetic “pseudo-tomographic” sections for models A and B, respectively, from 40 km to 400 km depth, using a wider colorbar scale (see text for details). Note in a) the low velocity anomaly located in the top-central part of the section, which can be correlated with the low-velocity anomaly created in our synthetic models by the crustal root and the hydrated mantle wedge on top of it. Note also the relatively flat surface at ~225 km depth where both types of sections show anomaly values around zero, separating a lower part with slow anomalies from an upper part with dominantly fast anomalies. d), plan view of the tomographic model of Chevrot et al. (2014), with anomalies averaged for depths between 125 and 150 km, after crustal correction. On top of this map, we have plotted the calculated anomalies of our synthetic models A and B for the same depth interval. Model A is depicted to the left and Model B to the right of the line marking the position of the transect. Calculated anomalies are lowered by 0.65% (see text for details). Note the E-W trending fast anomaly along the coast and the band to the south of relatively slow anomalies (between 42 and 43°N) that are spatially coincident with the lithospheric root and with the area of uplifted LAB, respectively, in our models.

depths (eg. Christensen and Mooney, 1995). Passive continental margins, both volcanic and magma-poor, often exhibit a layer of high seismic velocities ($V_p \approx 7.0\text{--}7.7 \text{ km s}^{-1}$) in the base of the crust that is generally interpreted as accumulated gabbroic intrusions (magmatic underplating) or upper mantle peridotites that were serpentinized when the overlying crust extended to the point that it became entirely brittle and seawater could penetrate into the mantle along faults. The distinction between these two end-members solely by their geophysical signatures is not easy, since both share the same range of P-wave velocity and density values, and strong magnetization (see, for example Mjelde et al. (2002) and references therein).

According to the interpretation of the North-Iberian margin made by Roca et al. (2011), this HVLC in the North-Iberian margin would correspond to lower continental crust as north as beneath Le Danois Bank,

and to exhumed upper mantle beneath the abyssal plain. During convergence, this serpentinized mantle would have been subducted to the south beneath the southern end of the abyssal plain, giving rise to the accretionary prism. The subduction plane would be the reactivation of the extensional detachment that led to mantle exhumation in the bay during the Mesozoic. We find several problems with this interpretation. First, there is no evidence for this subduction zone in the wide-angle models of both the ESCIN-4 and MARCONI-1 profiles. Rather, the wide-angle seismic recordings show a continuous Moho-like reflection in a flat surface located at the base of the supposedly serpentinized mantle layer (the HVLC), from north to south of Le Danois Bank (Fig. 3 and Supplementary Fig. 1a) and therefore cross-cutting the subduction plane in the reconstruction proposed by Roca et al. (2011). Also, the HVLC shows a very subtle vertical gradient of seismic velocities and

is limited by rather sharp boundaries, something that contrasts with the strong velocity gradients that are usually associated with serpentinization, a process that vanishes gradually with depth, giving rise to weak Moho reflections (eg. Dean et al., 2000). Since deformation started approximately at the same time or even earlier in the off-shore part of the belt than in the south-vergent part presently on-land, it would be also difficult to explain how and why deformation jumped from this weak zone of subduction that was easily accommodating the convergence, to a new completely independent subduction zone developed in the thicker continental crust.

Addition of mafic melts in the base of the crust is another process that is usually invoked to explain HVLC bodies. During the formation of any passive margin, even if it is of the “magma-poor” type, the lithospheric mantle will experience some amount of partial melting as a result of decompression. The amount of melt generated and the moment of appearance of this process with regard to serpentinization would mostly depend on rifting velocity, mantle composition and mantle potential temperature (Pérez-Gussinyé et al., 2006). Rifting velocities in the Bay of Biscay are difficult to estimate due to the rotational opening of the Bay and the disputed oceanic character and isochronism of the M0–M3 anomalies (Bronner et al., 2011, 2012; Tucholke and Sibuet, 2012). The most recent and undisputed anomalies in the center of the Bay (A330–A34) indicate half-spreading rates of 6.5 mm/yr, whereas lower rates of 3.3 mm/yr are calculated between A34 and M0 when M0 is considered as an isochron of Aptian age (118 Ma) (Sibuet et al., 2004). Numerical models predict that 2 to 4 km of melt thickness (depending on the position along the margin) is produced by decompression for half-spreading velocities between 4.2 and 6 mm/yr, and that this process occurs after mantle exhumation and its serpentinization (Pérez-Gussinyé et al., 2006). We consider that the HVLC most likely corresponds to stretched and thinned continental lower crust, mixed with serpentinized upper mantle and later intruded by mafic magmas generated by decompression melting. Some of these magmas found their way to the surface and are found as basaltic clasts in the Early Cretaceous syn-rift conglomerates of the Le Danois Bank (Capdevila et al., 1980), or forming volcanic edifices in the seafloor in nearby sections of the Armorican margin (Thinon et al., 2003). In the adjacent Basque-Cantabrian basin, magmatism led to a bathyal submarine volcanic system of alkali basaltic character and to a strong hydrothermal activity during the Albian to Santonian interval (Agirrezabala et al., 2013; Azambre and Rossy, 1976; Castañares et al., 2001). Addition of mafic magmas at the bottom of the crust and inside the serpentinized mantle can explain both the seismic velocities and the presence of Moho-like reflections, and this mechanism has been recently invoked to explain the origin of the M0–M3 magnetic anomalies in the Newfoundland-Iberia rift system (Bronner et al., 2011). On the other hand, completely fresh peridotites are not expected beneath this level of gabbroic underplating, and the velocities of 7.7–7.9 km s⁻¹ found beneath it can be explained by remnants of the deeper and less altered part of the formerly serpentinized mantle.

6.6. A tentative evolutionary model

Our Model B is consistent with the tectonic evolution proposed by Gallastegui (2000) and Gallastegui et al. (2002), implying about 96 km of shortening during the Alpine orogeny, and a crustal root extended down to depths of around 90 km. In the following we present an alternative model of evolution that gives rise to a shallower crustal-lithospheric root, compatible with the one considered in Model A. It is based on the same model but with some modifications inspired in the model of Sutra et al. (2013) for the West Iberian Margin. It also incorporates structural information provided by the MARCONI-1 profile and the results described and discussed in the previous sections. Fig. 12 illustrates the new model, with comparison to the one proposed by Gallastegui (2000).

During the Late Cretaceous, the North-Iberian margin was a wide margin, the continental platform extending well to the south in the present-day Duero basin, and the slope located in the present-day Le Danois Bank. The initial thermal structure at the onset of rifting in the Late Jurassic–Early Cretaceous must have been relatively cold, with temperatures at the Moho of 500–600 °C, as rifting affected the area ~150 Myr. after the Variscan orogenesis (Pérez-Gussinyé et al., 2003). During the rifting stage, upper crustal normal faults soled out in a weak decoupling horizon located in the middle crust, where temperatures corresponding to the onset of quartz and plagioclase plasticities are reached (300 °C and 450 °C, respectively) (Lavier and Manatschal, 2006; Sutra et al., 2013).

The brittle, uppermost mantle is affected by concave downward faults, also rooted in the mid-crustal detachment. These faults may force the localization of ductile shear in the lower crust, which is thinned and disrupted (Fig. 12a). The discontinuity of the lower crust in the transition from the continental platform to the slope (or between the proximal and necking domains, in more recent terminology, eg. Tugend et al. (2014)) is the main difference with the model of Gallastegui (2000), and is the one that allows us to propose a shallower crustal root in later stages.

When stretching factors reach values of $\beta = 3–5$, the whole crust is cold enough to become brittle (Pérez-Gussinyé and Reston, 2001), and the normal faults can exhumate lower crustal rocks that are eroded and resedimented in Early Cretaceous syn-rift conglomerates in the distal part of the continental slope (Capdevila et al., 1980). These faults provide paths also for the seawater to enter into the mantle and serpentinize it (Pérez-Gussinyé and Reston, 2001). Serpentinites are rheologically very weak (Escartín et al., 2001) and constitute the seaward continuation of the decoupling horizon. The Upper Cretaceous post-rift succession is very thin all along the margin (≤ 800 m), indicating that thermal subsidence was small. This must be related to the upwelling of hot asthenosphere and ascent of the hot products of decompression melting that affected the margin from Albian to Santonian times, the bulk of them produced after serpentinization, according to numerical modeling predictions (Pérez-Gussinyé et al., 2006). We interpret that these gabbroic melts intruded into the upper part of the serpentinized mantle creating the HVLC and a new seismic Moho at their base, in the contact with less hydrated mantle with velocities of 7.8–7.9 km s⁻¹. Note that in order to explain the great volume of hydrated mantle presently observed above the crustal root, and since we preclude significant water input from the subducting lower crust, we must consider that serpentinization locally reached depths close to 30 km, probably around faults affecting the brittle upper mantle (Fig. 12a). Although these great depths are not common, serpentinization down to 40 km depth has been proposed in other continental margins (Jiménez-Munt et al., 2010) and are supported by geochemical studies in ophiolites (Li and Lee, 2006). An alternative explanation would be that the zone of magmatic underplating may have been more restricted in the axis of the bay, being separated from the hyperthinned crustal domain by a band of serpentinized upper mantle (inset in Fig. 12a). This band could have been underthrust in an early stage of compressional deformation between the Late Cretaceous and the Early Eocene, until the new and relatively hot gabbroic lower crust found resistance to be underthrust and stacked against the thinned lower continental crust.

The paucity of thermal subsidence lasted until the main phase of compressional deformation started in the middle Eocene (Fig. 12b), indicating that complete thermal relaxation was not attained at that time, and the buoyancy of the new transitional crust would probably prevent it to sink into the mantle in a southward-directed subduction zone. Instead, the weak decoupling horizon located on top of the new HVLC would favor its underthrusting toward the south. It is well known that the *décollements* developed on top of serpentinized mantle are long-lived weakness zones that can even be enhanced by an increase in temperature (ie. heating from the gabbroic intrusions). Partial dehydration of the serpentinized mantle is possible, but would not have a significant

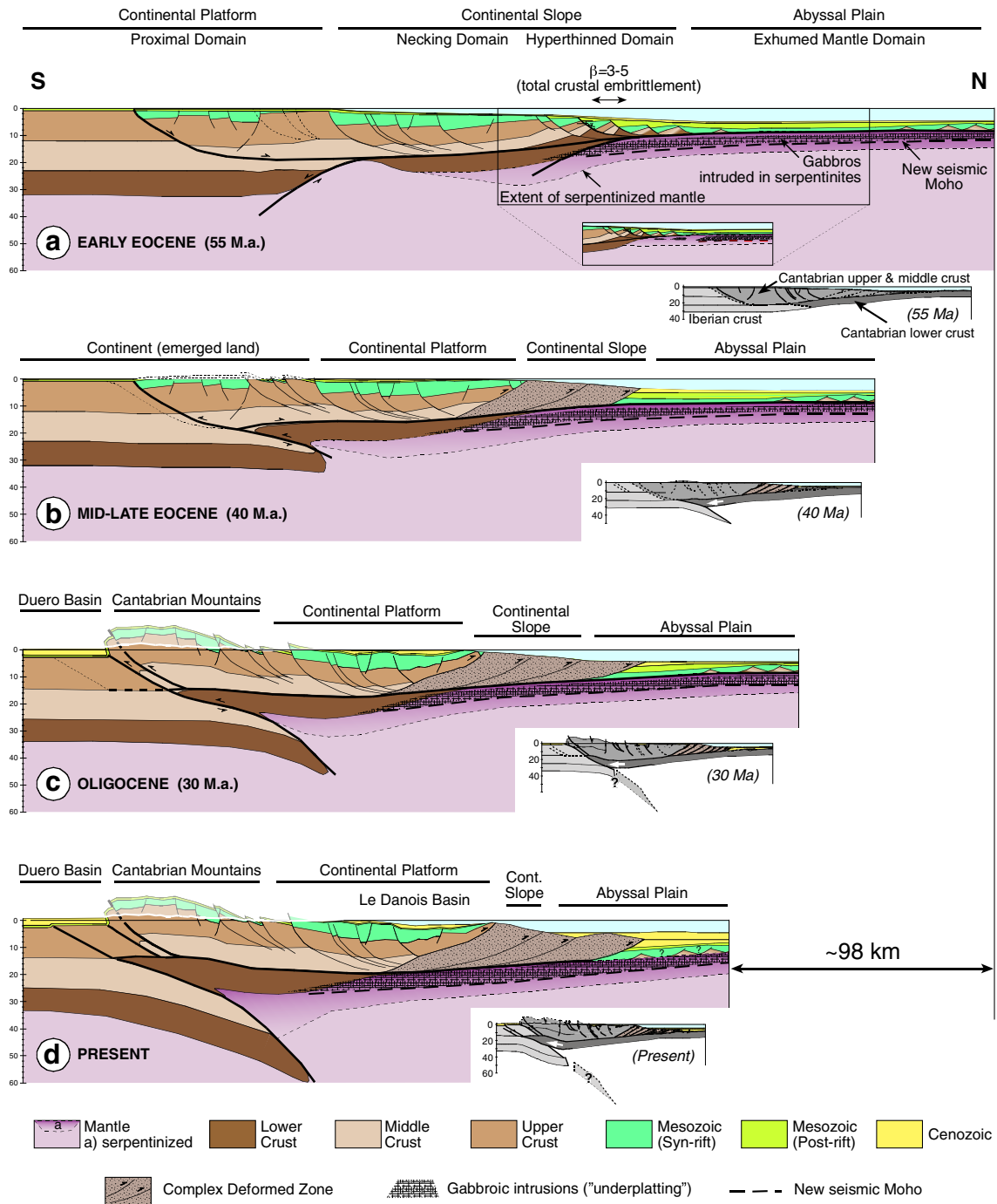


Fig. 12. Schematic Alpine tectonic evolution proposed for the studied transect. Equivalent stages in a previous model proposed by Gallastegui (2000) are included to the lower right of each panel for comparison. See Section 6.6 for details.

influence, since the presence of only 10% of serpentinite reduces the strength of the altered peridotite to that of nearly pure serpentinite (Escarot et al., 2001). Complete dehydration would require temperatures of 600 °C at 1–2 GPa, and even if serpentine minerals are dehydrated, talc is stable to ~800 °C at the same pressures, and has very low coefficients of friction (Lundin and Doré, 2011).

The underthrusting of the remnants of the lower continental crust of the margin and the new HVLC below this horizon promoted the development of north-directed thrust sheets on top of it, shortening the

continental platform and raising and steepening the continental slope (Fig. 12b). This “deformed area” (Gallastegui et al., 2002) involves sediments and basement rocks from all crustal levels. At the same time, the underthrusting of this lower crustal layer was accompanied by its indentation into the thicker part of the margin, splitting the Iberian crust along the former extensional detachment. This forced the beginning of an incipient subduction of the Iberian lower crust to the north (note that in the model by Gallastegui (2000) the root was already significant at this stage), and the uplift and subaerial exposure of the

former continental platform. Around ~40 Ma the continental sediments of the Oviedo basin were deposited onlapping southward over a karstified Cretaceous paleorelief (Alonso et al., 1996; Truyols and García Ramos, 1991). The lower crustal indentor progressed toward the south during the Oligocene (Fig. 12c), rising in the hangingwall of the former extensional detachment that bounded the syn-rift Mesozoic basin, and uplifting and exhuming the Variscan basement (Alonso et al., 1996). The Late Eocene–Oligocene age for the main exhumation phase of the Variscan basement along this transect is also corroborated by thermochronology studies (Fillon, 2012). The weak hydrated mantle beneath the lower crust of the margin was not able to indent and therefore began to be accreted against the subducting Iberian crust.

At some time between the Oligocene and the Early Miocene, the lower crustal wedge from the margin indented along a weakness horizon between the upper and middle crust of Iberia, perhaps following the sole thrust of the Variscan fold and thrust belt on top of the Precambrian basement (Pérez-Estaún et al., 1994). Since the Burdigalian (lower Miocene) deformation essentially came to an end (Alvarez-Marrón et al., 1997), and the mountain belt entered into an erosional phase.

The proposed evolutionary model allows us to explain several features of the present-day structure (Fig. 12d), such as the presence of high velocities in the lower crust of the North-Iberian margin gradually changing to “normal” lower crustal velocities toward the south, the high reflectivity character of the lower crust beneath the platform (Gallart et al., 1997) (generated by the gabbroic sills), the presence of a seismic Moho below the HVLC, and the low seismic velocities observed in the mantle beneath this Moho. Although a proper section balancing was not carried out, the dimensions of the crustal root and the southernmost position of the lower crustal indenting wedge beneath the mountain front allow us to infer a minimum shortening for the crust of ~98 km, approximately the same value proposed by Gallastegui (2000).

7. Conclusions

We present a seismically-constrained model of the lithospheric structure across the Cantabrian Mountains and the North-Iberian Margin that is able to explain the gravity anomalies, geoid undulations, surface heat flow and elevation over the area, as well as the lower crustal and upper mantle seismic velocities. The overall structure is the result of the Alpine compression acting on the Mesozoic passive continental margin. The lower crust from the necking and hyperthinned domains is interpreted to be indented southward into the proximal domain, forcing the shortening, uplift and exhumation of the former continental platform and the subduction to the north of the lower half of the crust. Two possible solutions are tested for the maximum depth extent of the Iberian crustal root: in Model A, it is limited to 60 km (only ~7 km more than the maximum depth the seismic experiments were able to resolve) and in Model B, it is extended down to ~90 km, as suggested in previous restored reconstructions (Gallastegui, 2000). The main results of this modeling can be summarized as follows:

1. From the geophysical point of view, both models A and B are feasible, but Model A is favored because it does not require to extrapolate the crustal root down to depths unconstrained by the seismic experiments, and its shallower lithospheric root fits slightly better with available tomographic results.
2. The Iberian lower crust is assumed to change its composition from dominantly felsic in the south to intermediate and hydrated (2 wt. %) in the area that will form the crustal root. The deepest part of the root is eclogitized, but it keeps all the water in the structure of hydrated minerals in the case of model A, and releases a small amount in the case of Model B (a maximum of ~0.8 wt% in the deepest part). Partial melt in the subducting lower crust is not expected, or it may occur in negligible amounts. If any melt was formed, it would be far from the critical percentage necessary to migrate and rise.

3. Low seismic velocities beneath the Bay of Biscay Moho and in the mantle wedge above the crustal root are explained by the addition of 1–2 wt% of water percolated from the seafloor during the formation of the margin in the Mesozoic. Water input from dehydration reactions in the subducting lower crust is ruled out in Model A and very minor in Model B (less than ~12% of the required water to hydrate the overlying mantle wedge with 1 wt % of water).
4. Assuming a composition typical for “tecton” garnet subcontinental lithospheric mantle (Griffin et al., 2009), the thickness of the thermal lithosphere varies from 125–145 km south of the Cantabrian Mountains, to 170 km beneath the crustal root (205 km in Model B) and 135–140 km beneath the central part of the Bay of Biscay. More enriched compositions such as those of some Pyrenean mantle xenoliths (Griffin et al., 2009; Le Roux et al., 2007) or the Primitive Upper Mantle of Jagoutz et al. (1979) were tested in Model A and allow a reduction of the lithospheric thickness of only ~5 km.
5. The upper mantle is interpreted to be serpentinized during the formation of the margin in the Mesozoic and later intruded by decompression melts generating a gabbroic underplating and a new seismic Moho at its base. We emphasize that the role of magmatism in ocean-continent transitions may be significant even in “non-volcanic margins”. During the Alpine convergence, these petrophysical transformations promoted the underthrusting and indentation to the south of the lower crust from the necking and hyperthinned domains (with the new gabbroic additions). This process is genetically linked to the uplift of the Cantabrian Mountains and the formation of a crustal root down to at least ~60 km depth, with an estimated crustal shortening of ~98 km.

Supplementary data to this article can be found online at <http://dx.doi.org/10.1016/j.lithos.2015.04.018>.

Acknowledgements

We thank Sébastien Chevrot and Antonio Villaseñor for providing the tomographic data, and Marco Scambelluri and two anonymous reviewers for their helpful comments and suggestions on earlier drafts of this manuscript. This is a contribution of the Consolider-Ingenio 2010 Project “Topo-Iberia” (CSD2006-00041), the European Science Foundation “Topo-Europe” Project “Spatial and temporal coupling between tectonics and surface processes during lithosphere inversion of the Pyrenean-Cantabrian Mountain belt (PYRTEC)” and the National R&D Plan Project TECLA (CGL2011-26670). Funding by the Government of Asturias (Spain) to Individual Project-2 within the PYRTEC project is greatly acknowledged. The work of JCA has been supported by an ARC Discovery Project grant (DP 120102372). This is contribution 580 from the ARC Centre of Excellence for Core to Crust Fluid Systems (<http://www.cfs.mq.edu.au>) and 987 in the GEMOC Key Centre (<http://www.gemoc.mq.edu.au>). Most of the figures were created using GMT software (Wessel and Smith, 1998).

References

- Afonso, J.C., Zlotnik, S., 2011. The subductability of continental lithosphere: the before and after story. *Arc-Continent Collision* 53–86.
- Afonso, J.C., Fernández, M., Ranalli, G., Griffin, W.L., Connolly, J.A.D., 2008. Integrated geophysical-petrological modeling of the lithosphere and sublithospheric upper mantle: Methodology and applications. *Geochemistry, Geophysics, Geosystems* 9, Q05008. <http://dx.doi.org/10.1029/2007GC001834>.
- Afonso, J.C., Fullea, J., Yang, Y., Connolly, J.A.D., Jones, A.G., 2013a. 3-D multi-observable probabilistic inversion for the compositional and thermal structure of the lithosphere and upper mantle. II: General methodology and resolution analysis. *Journal of Geophysical Research, Solid Earth* 118, 1650–1676. <http://dx.doi.org/10.1002/jgrb.50123>.
- Afonso, J.C., Fullea, J., Griffin, W.L., Yang, Y., Jones, A.G., D Connolly, J.A., O'Reilly, S.Y., 2013b. 3-D multiobservable probabilistic inversion for the compositional and thermal structure of the lithosphere and upper mantle. I: a prioripetrological information and geophysical observables. *Journal of Geophysical Research, Solid Earth* 118, 2586–2617. <http://dx.doi.org/10.1002/jgrb.50124>.

- Agirrezabala, L.M., Kiel, S., Blumenberg, M., Schäfer, N., Reitner, J., 2013. Outcrop analogues of pockmarks and associated methane-seep carbonates: A case study from the Lower Cretaceous (Albian) of the Basque-Cantabrian Basin, western Pyrenees. *Palaeogeography Palaeoclimatology Palaeoecology* 390, 94–115. <http://dx.doi.org/10.1016/j.palaeo.2012.11.020>.
- Alonso, J., Pulgar, J., García-Ramos, J., Barba, P., 1996. Tertiary basins and Alpine tectonics in the Cantabrian Mountains (NW Spain). Tertiary basins of Spain: the stratigraphic record of crustal kinematics. 6, 214.
- Álvarez-Marrón, J., Pérez-Estaún, A., Dañobeitia, J.J., Pulgar, J.A., Martínez Catalán, J.R., Marcos, A., Bastida, F., Ayarza-Arribas, P., Aller, J., Gallart, J., Gonzalez-Lodeiro, F., Banda, E., Comas, M.C., Córdoba, D., 1996. Seismic structure of the northern continental margin of Spain from ESCIN deep seismic profiles. *Tectonophysics* 264, 153–174.
- Alvarez-Marrón, J., Rubio, E., Tome, M., 1997. Subduction-related structures in the North Iberian margin. *Journal of Geophysical Research, Solid Earth* 102, 22497–22511.
- Artemieva, I.M., 2009. The continental lithosphere: Reconciling thermal, seismic, and petrologic data. *Lithos* 109, 23–46. <http://dx.doi.org/10.1016/j.lithos.2008.09.015>.
- Austrheim, H., Erambert, M., Engvik, A.K., 1997. Processing of crust in the root of the Caledonian continental collision zone: The role of eclogitization. *Tectonophysics* 273, 129–153.
- Ayala, C., 2013. A new compilation of gravity data over the Iberian Peninsula and surrounding areas. Internal Report Topo-Iberia Project (Consolider-Ingenio), IGME 1–20.
- Ayarza, P., Martínez-Catalán, J.R., Alvarez-Marrón, J., Zeyen, H., Juhlin, C., 2004. Geophysical constraints on the deep structure of a limited ocean-continent subduction zone at the North Iberian Margin. *Tectonics* 23. <http://dx.doi.org/10.1029/2002TC001487>.
- Azambre, B., Rossy, M., 1976. Le magmatisme alcalin d'âge crétacé dans les Pyrénées occidentales et l'Arc basque; ses relations avec le métamorphisme et la tectonique. *Bulletin de la Societe Geologique de France* 6, 1725–1728.
- Beaumont, C., Muñoz, J.A., Hamilton, J., Fullsack, P., 2000. Factors controlling the Alpine evolution of the central Pyrenees inferred from a comparison of observations and geodynamical models. *Journal of Geophysical Research* 105, 8121–8145.
- Boillot, G., Dupeuble, P.A., Malod, J., 1979. Subduction and tectonics on the continental margin off northern Spain. *Marine Geology* 32, 53–70.
- Bradley, D.C., 2008. Passive margins through earth history. *Earth-Science Reviews* 91, 1–26.
- Bronner, A., Sauter, D., Manatschal, G., Péron-Pinvidic, G., Munsch, M., 2011. Magmatic breakup as an explanation for magnetic anomalies at magma-poor rifted margins. *Nature Geoscience* 4, 549–553. <http://dx.doi.org/10.1038/nphys1201>.
- Bronner, A., Sauter, D., Manatschal, G., Péron-Pinvidic, G., Munsch, M., 2012. Problematic plate reconstruction. *Nature Geoscience* 5, 677. <http://dx.doi.org/10.1038/ngeo1597>.
- Brunet, M.F., 1994. Subsidence in the Parentis Basin (Aquitaine, France): Implications of the thermal evolution. In: Mascle, A. (Ed.), *Hydrocarbon and Petroleum Geology of France*. Special Publication of the European Association of Petroleum Geologists 4. Springer-Verlag, pp. 187–198.
- Capdevila, R., Boillot, G., Lepvrier, C., Malod, J.A., Mascle, G., 1980. Les formations cristallines du Banc Le Danois (marge nord-ibérique). *Comptes Rendus Académie des Sciences D* 291, 317–320.
- Carballo, A., Fernández, M., Torné, M., Jiménez-Munt, I., Villaseñor, A., 2015. Thermal and petrophysical characterization of the lithospheric mantle along the northeastern Iberia geo-transect. *Gondwana Research* 27 (4), 1430–1445.
- Carlson, R.L., 2003. Mantle wedge water contents estimated from seismic velocities in partially serpentinized peridotites. *Geophysical Research Letters* 30, 1250. <http://dx.doi.org/10.1029/2002GL016600>.
- Casanovas-Cladellas, M.L., Jiménez Fuentes, E., Martín-Closas, C., Moyá-Solá, S., Santafé-Llopis, J.V., Truyols, J., 1991. Consideraciones sobre la edad del yacimiento Eocénico de Llamaquique (Oviedo, España). *Boletín de Ciencias de la Naturaleza. I.D.E.A.*, pp. 253–261.
- Casas, A., Kearey, P., Rivero, L., Adam, C., 1997. Gravity anomaly map of the Pyrenean region and a comparison of the deep geological structure of the western and eastern Pyrenees. *Earth and Planetary Science Letters* 150, 65–78.
- Castañares, L.M., Robles, S., Gimeno, D., Bravo, J.C.V., 2001. The submarine volcanic system of the Errigoiti Formation (Albian-Santonian of the Basque-Cantabrian Basin, Northern Spain): stratigraphic framework, facies, and sequences. *Journal of Sedimentary Research* 71, 318–333.
- Chapman, D., 1986. Thermal gradients in the continental crust. In: Dawson, J., et al. (Eds.), *The Nature of the Lower Continental Crust*. Geological Society Special Publication 24, pp. 63–70.
- Chevrot, S., Villaseñor, A., Sylvander, M., Benahmed, S., Beucler, E., Cougoulat, G., Delmas, P., Saint Blanquat, M. (de), Diaz, J., Gallart, J., Grimaud, F., Lagabrielle, Y., Manatschal, G., Mocquet, A., Pauchet, H., Paul, A., Péquignat, C., Quillard, O., Roussel, S., Ruiz, M., Wolyniec, D., 2014. High-resolution imaging of the Pyrenees and Massif Central from the data of the PYROPE and IBERARRAY portable array deployments. *J. Geophys. Res. Solid Earth* 119. <http://dx.doi.org/10.1002/2014JB010953>.
- Christensen, N.I., Mooney, W.D., 1995. Seismic velocity structure and composition of the continental crust: A global view. *Journal of Geophysical Research* 100, 9761.
- Clauser, C., Huenges, E., 1995. Thermal conductivity of rocks and minerals. In: Ahrens, T.J. (Ed.), *A Handbook of Physical Constants: Rock Physics and Phase Relations*. American Geophysical Union, pp. 105–126.
- Connolly, J.A.D., 2005. Computation of phase equilibria by linear programming: A tool for geodynamic modeling and its application to subduction zone decarbonation. *Earth and Planetary Science Letters* 236, 524–541. <http://dx.doi.org/10.1016/j.epsl.2005.04.033>.
- Connolly, J.A.D., 2009. The geodynamic equation of state: What and how. *Geochemistry, Geophysics, Geosystems* 10, Q10014. <http://dx.doi.org/10.1029/2009GC002540>.
- Dean, S.M., Minshull, T.A., Whitmarsh, R.B., Loudon, K.E., 2000. Deep structure of the ocean–continent transition in the southern Iberia Abyssal Plain from seismic refraction profiles: The IAM-9 transect at 40° 20' N. *Journal of Geophysical Research: Solid Earth* (1978–2012) 105, 5859–5885.
- Engvik, A.K., Austrheim, H., Erambert, M., 2001. Interaction between fluid flow, fracturing and mineral growth during eclogitization, an example from the Sunnfjord area, Western Gneiss Region, Norway. *Lithos* 57, 111–141.
- Escartín, J., Hirth, G., Evans, B., 2001. Strength of slightly serpentinized peridotites: Implications for the tectonics of oceanic lithosphere. *Geology* 29, 1023. [http://dx.doi.org/10.1130/0091-7613\(2001\)029<1023:SOSSPI>2.0.CO;2](http://dx.doi.org/10.1130/0091-7613(2001)029<1023:SOSSPI>2.0.CO;2).
- Fariás, P., Gallastegui, G., González-Lodeiro, F., Marquínez, J., Parra, L.M.M., Catalán, J.R.M., de Pablo Maciá, J.G., Fernández, L.R.R., 1987. Aportaciones al conocimiento de la litoestratigrafía y estructura de Galicia Central. *Memórias da Faculdade de Ciências da Universidade do Porto* 1, 411–431.
- Fernández, M., Marzán, I., Correia, A., Ramalho, E., 1998. Heat flow, heat production, and lithospheric thermal regime in the Iberian Peninsula. *Tectonophysics* 291, 29–53.
- Fernández-Viejo, G., 1997. Estructura cortical de la Cordillera Cantábrica y su transición a la Cuenca del Duero a partir de datos de sismica de refracción/reflexión de gran ángulo. PhD Thesis, Univ. Barcelona (309 pp.).
- Fernández-Viejo, G., Gallart, J., Pulgar, J.A., Gallastegui, J., Dañobeitia, J.J., Córdoba, D., 1998. Crustal transition between continental and oceanic domains along the North Iberian margin from wide angle seismic and gravity data. *Geophysical Research Letters* 25, 4249–4252.
- Fernández-Viejo, G., Gallart, J., Pulgar, J.A., Córdoba, D., Dañobeitia, J.J., 2000. Seismic signature of Variscan and Alpine tectonics in NW Iberia: Crustal structure of the Cantabrian Mountains and Duero basin. *Journal of Geophysical Research: Solid Earth* (1978–2012) 105, 3001–3018.
- Fernández-Viejo, G., Pulgar, J.A., Gallastegui, J., Quintana, L., 2012. The Fossil Accretionary Wedge of the Bay of Biscay: Critical Wedge Analysis on Depth-Migrated Seismic Sections and Geodynamical Implications. *The Journal of Geology* 120, 315–331. <http://dx.doi.org/10.1086/664789>.
- Fillon, C., 2012. Spatial and temporal variations in Cenozoic exhumation of the Pyrenean-Cantabrian mountain belt: coupling between tectonics and surface processes. PhD Thesis, Univ. Grenoble-Univ. Bergen (201 pp.).
- Fouliquer, G.R., Panza, G.F., Artemieva, I.M., Bastow, I.D., Cammarano, F., Evans, J.R., Hamilton, W.B., Julian, B.R., Lustrino, M., Thybo, H., Yanovskaya, T.B., 2013. Caveats on tomographic images. *Terra Nova* 25, 259–281. <http://dx.doi.org/10.1111/ter.12041>.
- Früh-Green, G.L., Connolly, J.A., Plas, A., Kelley, D.S., Gröbety, B., 2004. Serpentinization of oceanic peridotites: implications for geochemical cycles and biological activity. *Geophysical Monograph Series* 144, 119–136.
- Fullea, J., Fernández, M., Zeyen, H., 2008. FA2BOUG—A FORTRAN 90 code to compute Bouguer gravity anomalies from gridded free-air anomalies: Application to the Atlantic-Mediterranean transition zone. *Computers and Geosciences* 34, 1665–1681. <http://dx.doi.org/10.1016/j.cageo.2008.02.018>.
- Fullea, J., Fernández, M., Afonso, J.C., Verges, J., Zeyen, H., 2010. The structure and evolution of the lithosphere–asthenosphere boundary beneath the Atlantic–Mediterranean Transition Region. *Lithos* 120 (1–2), 74–95.
- Gallart, J., Fernández-Viejo, G., Diaz, J., Vidal, N., Pulgar, J.A., 1997. Deep structure of the transition between the Cantabrian Mountains and the north Iberian Margin from wide-angle ESCI-N data. *Revista de la Sociedad Geológica de España* 8 (4), 365–382.
- Gallastegui, J., 2000. Estructura cortical de la cordillera y margen continental Cantábricos: Perfiles ESCI-N. *Trabajos de Geología* 22, 3–234.
- Gallastegui, J., Pulgar, J.A., Gallart, J., 2002. Initiation of an active margin at the North Iberian continent-ocean transition. *Tectonics* 21, 15–15–14.
- García-Castellanos, D., Fernández, M., Torne, M., 1997. Numerical modeling of foreland basin formation: a program relating thrusting, flexure, sediment geometry and lithosphere rheology. *Computers and Geosciences* 23, 993–1003.
- Griffin, W.L., O'Reilly, S.Y., Afonso, J.C., Begg, G.C., 2009. The Composition and Evolution of Lithospheric Mantle: a Re-evaluation and its Tectonic Implications. *Journal of Petrology* 50, 1185–1204. <http://dx.doi.org/10.1093/petrology/egn033>.
- Gutiérrez Alonso, G., Johnston, S.T., Weil, A.B., Pastor-Galán, D., Fernández-Suárez, J., 2012. Buckling an orogen: The Cantabrian Orocline. *GSA Today* 4–9 <http://dx.doi.org/10.1130/GSATG141A.1>.
- Hofmeister, A.M., 1999. Mantle Values of Thermal Conductivity and the Geotherm from Phonon Lifetimes. *Science* 283, 1699–1706. <http://dx.doi.org/10.1126/science.283.5408.1699>.
- Holland, T., Powell, R., 1998. An internally consistent thermodynamic data set for phases of petrological interest. *Journal of Metamorphic Geology* 16, 309–343.
- Holland, T., Powell, R., 2001. Calculation of phase relations involving haplogranitic melts using an internally consistent thermodynamic dataset. *Journal of Petrology* 42, 673–683.
- Huismans, R.S., Beaumont, C., 2007. Roles of lithospheric strain softening and heterogeneity in determining the geometry of rifts and continental margins. *Geological Society, London, Special Publications* 282, 111–138. <http://dx.doi.org/10.1144/SP282.6>.
- Huismans, R., Beaumont, C., 2011. Depth-dependent extension, two-stage breakup and cratonic underplating at rifted margins. *Nature* 473, 74–78. <http://dx.doi.org/10.1038/nature09988>.
- Hung, S.H., Dahlen, F.A., Nolet, G., 2001. Wavefront healing: A banana-doughnut perspective. *Geophysical Journal International* 146, 289–312.
- Hyndman, R.D., Shearer, P.M., 1989. Water in the lower continental crust: modelling magnetotelluric and seismic reflection results. *Geophysical Journal International* 98, 343–365.
- Jagoutz, E., Palme, H., Baddenhausen, H., Blum, K., Cendales, M., Dreibus, G., Spettel, B., Lorenz, V., Wanke, H., 1979. The abundance of major, minor and trace elements in the Earth's mantle as derived from primitive ultramafic nodules. *Proceedings of the 10th Lunar and Planetary Science Conference. Geochimica et Cosmochimica Acta Supplement* 2031–2050.

- Jammes, S., Huisman, R.S., Muñoz, J.-A., 2014. Lateral variation in structural style of mountain building: controls of rheological and rift inheritance. *Terra Nova* 26, 201–207. <http://dx.doi.org/10.1111/ter.12087>.
- Jiménez-Díaz, A., Ruiz, J., Villaseca, C., Tejero, R., Capote, R., 2012. The thermal state and strength of the lithosphere in the Spanish Central System and Tajo Basin from crustal heat production and thermal isostasy. *Journal of Geodynamics* 58, 29–37. <http://dx.doi.org/10.1016/j.jog.2012.01.005>.
- Jiménez-Munt, I., Fernández, M., Vergés, J., Afonso, J.C., García-Castellanos, D., Fulla, J., 2010. Lithospheric structure of the Gorringe Bank: Insights into its origin and tectonic evolution. *Tectonics* 29, TC5019. <http://dx.doi.org/10.1029/2009TC002458>.
- Julivert, M., Fontboté, J.M., Ribeiro, A., Conde, L.E., 1972. Mapa tectónico de la Península Ibérica y Baleares, E: 1:1.000.000. *Ins. Geol. Min. Esp.*
- Kennett, B.L.N., Engdahl, E.R., Buland, R., 1995. Constraints on seismic velocities in the Earth from traveltimes. *Geophysical Journal International* 122, 108–124.
- Lavier, L.L., Manatschal, G., 2006. A mechanism to thin the continental lithosphere at magma-poor margins. *Nature* 440, 324–328. <http://dx.doi.org/10.1038/nature04608>.
- Le Pichon, X., Bonnin, J.C., Francheteau, J., Sibuet, J.C., 1971. Une hypothèse d'évolution tectonique du Golfe de Gascogne. In: Debysier, J., Le Pichon, X., Montadert, M. (Eds.), *Histoire structurale du Golfe de Gascogne*. Technip, Paris, pp. VI.11.1–VI.11.44.
- Le Roux, V., Bodinier, J.L., Tommasi, A., Alard, O., Dautria, J.M., Vauchez, A., Riches, A.J.V., 2007. The Lherz spinel lherzolite: Refertilized rather than pristine mantle. *Earth and Planetary Science Letters* 259, 599–612. <http://dx.doi.org/10.1016/j.epsl.2007.05.026>.
- Li, Z.-X.A., Lee, C.-T.A., 2006. Geochemical investigation of serpentinized oceanic lithospheric mantle in the Feather River Ophiolite, California: Implications for the recycling rate of water by subduction. *Chemical Geology* 235, 161–185. <http://dx.doi.org/10.1016/j.chemgeo.2006.06.011>.
- Ludwig, J.W., Nafe, J.E., Drake, C.L., 1970. In: Maxwell, A. (Ed.), *Seismic refraction. The Sea vol. 4*. John Wiley, Hoboken, N. J., pp. 53–84.
- Lundin, E.R., Doré, A.G., 2011. Hyperextension, serpentinization, and weakening: A new paradigm for rifted margin compressional deformation. *Geology* 39, 347–350. <http://dx.doi.org/10.1130/G31499.1>.
- Manatschal, G., Lavier, L., Chenin, P., 2015. The role of inheritance in structuring hyperextended rift systems: Some considerations based on observations and numerical modeling. *Gondwana Research* 27, 140–164. <http://dx.doi.org/10.1016/j.gr.2014.08.006>.
- Matte, P., 1991. Accretionary history and crustal evolution of the Variscan belt in Western Europe. *Tectonophysics* 196, 309–337.
- McDonough, W.F., Sun, S.S., 1995. The composition of the Earth. *Chemical Geology* 120, 223–253.
- Mendia, M.S., Ibarra, J.I.G., 1991. High-grade metamorphic rocks and peridotites along the Leiza Fault (Western Pyrenees, Spain). *Geologische Rundschau* 80, 93–107.
- Missenard, Y., Cadoux, A., 2012. Can Moroccan Atlas lithospheric thinning and volcanism be induced by Edge-Driven Convection? *Terra Nova* 24 (1), 27–33. <http://dx.doi.org/10.1111/j.1365-3121.2011.01033.x>.
- Mjelde, R., Kasahara, J., Shimamura, H., Kamimura, A., Kanazawa, T., Kodaira, S., Raum, T., Shiobara, H., 2002. Lower crustal seismic velocity-anomalies; magmatic underplating or serpentinized peridotite? Evidence from the Vøring Margin, NE Atlantic. *Marine Geophysical Research* 23, 169–183.
- Muñoz, J.A., 2002. Alpine tectonics I: The Alpine system north of the Beltic Cordillera: The Pyrenees. In: Gibbons, W., Moreno, T. (Eds.), *The Geology of Spain*. Geol. Soc. London, pp. 370–385.
- Pavlis, N.K., Holmes, S.A., Kenyon, S.C., Factor, J.K., 2012. The development and evaluation of the Earth Gravitational Model 2008 (EGM2008). *Journal of Geophysical Research* 117, B04406. <http://dx.doi.org/10.1029/2011JB008916>.
- Pedreira, D., Pulgar, J., Gallart, J., Díaz, J., 2003. Seismic evidence of Alpine crustal thickening and wedging from the western Pyrenees to the Cantabrian Mountains (north Iberia). *Journal of Geophysical Research* 108, 2204.
- Pedreira, D., Pulgar, J.A., Gallart, J., Torne, M., 2007. Three-dimensional gravity and magnetic modeling of crustal indentation and wedging in the western Pyrenees-Cantabrian Mountains. *Journal of Geophysical Research* 112. <http://dx.doi.org/10.1029/2007JB005021>.
- Pedreira, D., Ebbing, D., Pulgar, J.A., 2010. Lithospheric structure of the Western Pyrenees-Cantabrian Mountains based on 3D modelling of gravity anomalies and geoid undulations: preliminary results. *Trabajos de Geología* 30, 121–127.
- Pérez-Estaún, A., Martínez-Catalán, J.R., Bastida, F., 1991. Crustal thickening and deformation sequence in the footwall to the suture of the Variscan belt of northwest Spain. *Tectonophysics* 191, 243–253.
- Pérez-Estaún, A., Pulgar, J.A., Banda, E., Alvarez-Marrón, J., ESCI-N Research Group, 1994. Crustal structure of the external variscides in northwest Spain from deep seismic reflection profiling. *Tectonophysics* 232 (91–112), 115–118.
- Pérez-Gussinyé, M., Reston, T.J., 2001. Rheological evolution during extension at nonvolcanic rifted margins: onset of serpentinization and development of detachments leading to continental breakup. *Journal of Geophysical Research: Solid Earth* (1978–2012) 106, 3961–3975.
- Pérez-Gussinyé, M., Watts, A.B., 2005. The long-term strength of Europe and its implications for plate-forming processes. *Nature* 436, 381–384.
- Pérez-Gussinyé, M., Ranero, C.R., Reston, T.J., Sawyer, D., 2003. Mechanisms of extension at nonvolcanic margins: Evidence from the Galicia interior basin, west of Iberia. *Journal of Geophysical Research, B: Solid Earth* 108, 6-1–6-19 (EPM).
- Pérez-Gussinyé, M., Morgan, J.P., Reston, T.J., Ranero, C.R., 2006. The rift to drift transition at non-volcanic margins: Insights from numerical modelling. *Earth and Planetary Science Letters* 244, 458–473.
- Pulgar, J.A., Gallart, J., Fernández-Viejo, G., Pérez-Estaún, A., Alvarez-Marrón, J., ESCIN Group, 1996. Seismic image of the Cantabrian Mountains in the western extension of the Pyrenees from integrated ESCIN reflection and refraction data. *Tectonophysics* 264, 1–19.
- Pulgar, J.A., Pérez-Estaún, A., Gallart, J., Alvarez-Marrón, J., Alonso, J.L., Group, E., 1997. The ESCI-N2 deep seismic reflection profile: a traverse across the Cantabrian Mountains and adjacent Duero basin. *Revista de la Sociedad Geológica de España* 8, 383–394.
- Quintana, L., 2012. *Extensión e Inversión Tectónica en el sector central de la Región Vasco-Cantábrica (Cantabria-Vizcaya, norte de España)*. Unpublished PhD Thesis, Universidad de Oviedo, Spain (560 pp, 2 maps and 5 cross-section plates).
- Roca, E., Muñoz, J.-A., Ferrer, O., Ellouz, N., 2011. The role of the Bay of Biscay Mesozoic extensional structure in the configuration of the Pyrenean orogen: Constraints from the MARCONI deep seismic reflection survey. *Tectonics* 30, TC2001. <http://dx.doi.org/10.1029/2010TC002735>.
- Rodríguez Fernández, L.R., Bellido, F., Díez Montes, A., Gallastegui, G., González Clavijo, E., López Olmedo, F., Marin, C., Martín Parra, L.M., Martín Serrano, A., Matas, J., Montes, M., Nozal, F., Roldán, F., Rubio, F., 2004. Mapa Geológico de España, E:1:2.000.000. IGME.
- Rosenberg, C.L., Handy, M.R., 2005. Experimental deformation of partially melted granite revisited: implications for the continental crust. *Journal of Metamorphic Geology* 23, 19–28. <http://dx.doi.org/10.1111/j.1525-1314.2005.00555.x>.
- Rudnick, R.L., Fountain, D.M., 1995. Nature and composition of the continental crust: a lower crustal perspective. *Reviews of Geophysics* 33, 267–309.
- Rudnick, R.L., Gao, S., 2003. Composition of the continental crust. In: Rudnick, R.L., Holland, H.D., Turekian, K.K. (Eds.), *Treatise on Geochemistry. The Crust vol. 3*. Elsevier, Oxford, pp. 1–64.
- Ruiz, M., 2007. *Caracterització estructural i sismotectònica de la litosfera en el domini Pirenaic-Cantàbric a partir de mètodes de sísmica activa i passiva*. Univ. Barcelona, pp. 1–354 (PhD Thesis).
- Ruiz, M., Díaz, J., Gallart, J., Pedreira, D., Pulgar, J.A., 2015. Seismic structure of the North-Iberian continental margin from wide-angle data of the MARCONI project (in prep.).
- Sandwell, D.T., Smith, W.H.F., 2009. Global marine gravity from retracked Geosat and ERS-1 altimetry: Ridge segmentation versus spreading rate. *Journal of Geophysical Research* 114, B01411. <http://dx.doi.org/10.1029/2008JB006008>.
- Semprich, J., Simon, N.S.C., Podladchikov, Y.Y., 2010. Density variations in the thickened crust as a function of pressure, temperature, and composition. *International Journal of Earth Sciences* 99, 1487–1510. <http://dx.doi.org/10.1007/s00531-010-0557-7>.
- Sibuet, J.-C., Srivastava, S.P., Spakman, W., 2004. Pyrenean orogeny and plate kinematics. *Journal of Geophysical Research* 109. <http://dx.doi.org/10.1029/2003JB002514>.
- Smith, W.H.F., Sandwell, D.T., 1997. Global Sea Floor Topography from Satellite Altimetry and Ship Depth Soundings. *Science* 277, 1956–1962. <http://dx.doi.org/10.1126/science.277.5334.1956>.
- Sutra, E., Manatschal, G., Mohn, G., Unternehr, P., 2013. Quantification and restoration of extensional deformation along the Western Iberia and Newfoundland rifted margins. *Geochemistry, Geophysics, Geosystems* 14, 2575–2597. <http://dx.doi.org/10.1002/ggge.20135>.
- Talwani, M., Worzel, J., Landisman, L., 1959. Rapid computations for two-dimensional bodies with application to the Mendocino submarine fracture zone. *Journal of Geophysical Research* 64, 49–59.
- Thinon, I., Matias, L., Réhault, J.-P., Hirn, A., Fidalgo-González, L., Avedik, F., 2003. Deep structure of the Armorican Basin (Bay of Biscay): a review of Norgasis seismic reflection and refraction data. *Journal of the Geological Society* 160, 99–116.
- Torne, M., De Cabissole, B., Bayer, R., Casas, A., Daignières, M., Rivero, A., 1989. Gravity constraints on the deep structure of the Pyrenean belt along the ECORS profile. *Tectonophysics* 165, 105–116.
- Truyols, J., García Ramos, J.C., 1991. El Terciario de la cuenca de Oviedo y el yacimiento de vertebrados de Llamaquique. *Boletín de Ciencias de la Naturaleza*. I.D.E.A., pp. 77–99.
- Tucholke, B.E., Sibuet, J.-C., 2012. Problematic plate reconstruction. *Nature Geoscience* 5, 676–677. <http://dx.doi.org/10.1038/ngeo1596>.
- Tugend, J., Manatschal, G., Kusznir, N.J., Masini, E., Mohn, G., Thinon, I., 2014. Formation and deformation of hyperex-tended rift systems: Insights from rift domain mapping in the Bay of Biscay- Pyrenees. *Tectonics* 33. <http://dx.doi.org/10.1002/2014TC003529>.
- Vielzeuf, D., 1984. Relations de phases dans le faciès granulite et implications géodynamiques: l'exemple des granulites des Pyrénées. *Université de Clermont-Ferrand II*.
- Vilà, M., Fernández, M., Jiménez-Munt, I., 2010. Radiogenic heat production variability of some common lithological groups and its significance to lithospheric thermal modeling. *Tectonophysics* 490, 152–164. <http://dx.doi.org/10.1016/j.tecto.2010.05.003>.
- Villaseca, C., Downes, H., Pin, C., Barbero, L., 1999. Nature and composition of the lower continental crust in Central Spain and the granulite-granite linkage: Inferences from granulitic xenoliths. *Journal of Petrology* 40, 1465–1496.
- Villaseñor, A., Spakman, W., Engdahl, E.R., 2003. Influence of regional travel times in global tomographic models. *Geophysical Research Abstracts*. EAE03-A-08614, EGS- AGU-EUG Joint Assembly, Nice, France, vol. 5.
- Vissers, R.L.M., Meijer, P.T., 2012. Iberian plate kinematics and Alpine collision in the Pyrenees. *Earth-Science Reviews* 114, 61–83. <http://dx.doi.org/10.1016/j.earscirev.2012.05.001>.
- Vosteen, H.-D., Schellschmidt, R., 2003. Influence of temperature on thermal conductivity, thermal capacity and thermal diffusivity for different types of rock. *Physics and Chemistry of the Earth, Parts A/B/C* 28, 499–509. [http://dx.doi.org/10.1016/S1474-7065\(03\)00069-X](http://dx.doi.org/10.1016/S1474-7065(03)00069-X).
- Watts, A.B., 2001. *Isostasy and Flexure of the Lithosphere*. Cambridge University Press, Cambridge, UK.
- White, R.W., 2001. *Isostasy and Flexure of the Lithosphere*. Cambridge University Press, Cambridge, UK.

- White, R.W., Powell, R., Holland, T.J.B., 2001. Calculation of partial melting equilibria in the system Na₂O–CaO–K₂O–FeO–MgO–Al₂O₃–SiO₂–H₂O (NCKFMASH). *Journal of Metamorphic Geology* 19, 139–153.
- Wilson, J.T., 1966. Did the Atlantic close and then re-open? *Nature* 211, 676–681. <http://dx.doi.org/10.1038/211676a0>.
- Zarnek, S.E., Parmentier, E.M., 2004. The onset of convection in fluids with strongly temperature-dependent viscosity cooled from above with implications for planetary lithospheres. *Earth and Planetary Science Letters* 224, 371–386.
- Zeyen, H., Ayarza, P., Fernández, M., Rimi, A., 2005. Lithospheric structure under the western African-European plate boundary: A transect across the Atlas Mountains and the Gulf of Cadiz. *Tectonics* 24, TC2001. <http://dx.doi.org/10.1029/2004TC001639>.
- Zlotnik, S., Afonso, J.C., Díez, P., Fernández, M., 2008. Small-scale gravitational instabilities under the oceans: implications for the evolution of oceanic lithosphere and its expression in geophysical observables. *Philosophical Magazine* 88, 3197–3217. <http://dx.doi.org/10.1080/14786430802464248>.

Geophysical-petrological modeling of the lithosphere beneath the Cantabrian Mountains and the North-Iberian margin: geodynamic implications

David Pedreira, Juan Carlos Afonso, Javier A. Pulgar, Jorge Gallastegui, Alberto Carballo, Manel Fernández, Daniel Garcia-Castellanos, Ivone Jiménez-Munt, Julia Semprich and Olga García-Moreno

doi:10.1016/j.lithos.2015.04.018

Supplementary Information

S1. Geophysical constraints on the crustal structure

The crustal structure of the model is constrained by a wide range of geological and geophysical data, such as oil exploration wells, isobath maps, commercial seismic lines, and deep seismic reflection and refraction/wide-angle reflection profiles.

Starting from top to bottom, the architecture of the Mesozoic-Cenozoic basins is relatively well constrained due to the large number of oil exploration data (seismic lines and wells) available in this region. The geometry of the off-shore Le Danois basin was taken from Gallastegui et al. (2002) and Cadenas (2013), and the base of the Duero basin is based on published isobath maps constrained by a network of seismic profiles and wells (Gallastegui, 2000, Heredia et al., 2010). Only the southernmost part of the Duero basin, where there are no data available, has been slightly modified from those maps to fit the Bouguer anomalies.

The northern limit of the Duero Basin is marked by the southern frontal structure of the Cantabrian Mountains, which has been clearly imaged by several commercial seismic lines down to ~2 s two-way travel time (TWTT) (Gallastegui, 2000). The ESCIN-2 seismic reflection profile across the central Cantabrian Mountains (Pulgar et al., 1996; 1997) provides a clear image of this structure down to 5-6 s TWTT, where it

roots into a flat horizontal level (Figure 3 of main article). Beneath this level, a wedge-shaped area with strong subhorizontal reflectors is clearly identified, thinning towards the South (orange shaded in Figure 3, upper left panel). The reflectivity of the crust beneath 6 s TWTT is highly variable, but it is clearly subhorizontal beneath the Duero basin, and North-dipping from the mountain front to the North (blue shaded in Figure 3), beneath the wedge-shaped area of strong subhorizontal reflectors. Note that the blue shaded zone in Figure 3 must correspond to the middle and lower crust of Iberia, according to the information provided by the seismic refraction profile 5 (Figure 3, lower panel).

The Iberian Moho is identified at 11.5-12 s TWTT beneath the Duero basin, and starts dipping towards the North beneath the Cantabrian Mountains, down to ~15 s TWTT in the northern end of the profile (located 30 km South of the coastline). Normal-incidence ray-tracing modeling carried out by Gallastegui (2000) locate the Moho at 34 km depth beneath the Duero Basin and at 42 km depth in the northernmost point sampled by the reflections, which due to its dipping attitude, corresponds to a point at ~17 km to the South of the northern edge of the profile. However, the wide-angle reflections recorded by 7 land stations deployed in a N-S line during the acquisition of the marine ESCIN-4 profile (see location in Figure 2) provided clear evidence for the continuity of the Iberian Moho down to at least ~53 km. As documented by Pulgar et al. (1996), Gallart et al. (1997) and Fernández-Viejo et al. (1998), the northernmost stations (located very close to the coastline) only recorded one strong reflection, identified as the reflection at the Moho (PmP) beneath the Cantabrian margin (and continuing about 10-15 km inland), whereas stations to the South also imaged another strong reflection produced in a deeper, North-dipping discontinuity, interpreted to be the subducting Iberian Moho (Supplementary Figure 1a). Ray-tracing

modeling locates the “Cantabrian Moho” at 30 km depth beneath the coastline, uprising to ~16-18 beneath the abyssal plain. The “Iberian” Moho, on the other hand, is located at 48-53 km depth, some 15-20 km to the South of the coastline.

Wide-angle recordings of the off-shore MARCONI-1 seismic profile, located approximately along the studied transect (Figure 2), also provided similar results (Ruiz, 2007; Ruiz et al., in prep.). Again, the maximum depth of the subducted crust could not be resolved. However, ocean bottom seismometers and wide-angle recordings on land provided valuable constraints on the crustal thickness in the margin and on the velocity of P-waves traveling through the upper mantle (P_n phase, Supplementary Figure 1b and c). The resulting velocities of 7.70-7.90 km s⁻¹ are too low to be caused by compositional or realistic thermal anomalies, and the easiest way to explain them is considering that the upper mantle is partly hydrated/serpentinized.

Unfortunately, due to the geometry of the seismic deployment, it was also not possible to obtain a good image of the internal structure of the crust in a wide strip beneath the coastline. Gravity data, however, provide additional constraints. The fact that the Bouguer anomaly increases continuously from the Duero Basin to the North over the crustal root suggests that some dense material must be present in the thickened part of the crust; otherwise the extra crustal thickness would create a regional minimum in the gravity anomaly map. 2D and 3D gravity models (Fernández-Viejo et al., 1998; Gallastegui, 2000; Pedreira et al., 2007) have shown that the anomaly can be easily fit assuming typical lower crustal densities for the wedge-shaped area of strong subhorizontal reflections observed in the northern part of the ESCIN-2 profile. This “indenter” is located at depths that are also compatible with a relative increment in the P-wave velocity along an E-W trending seismic refraction/wide-angle reflection profile (Fernández-Viejo et al., 2000; Pedreira et al., 2003, 2007). All these geophysical

signatures (strong reflectivity, high density and relatively high seismic velocities) point to a lower crustal composition for this wedge. The aforementioned constraints indicate that it can be easily associated with the lower crust of the Cantabrian margin (Gallastegui, 2000), which would be indented into the Iberian crust, forcing its northward subduction. This requires a detachment level on top of the lower crust of the Cantabrian margin, which would also explain the stacking of sedimentary units forming accretionary prism-like structures at the foot of the continental slope (Fernández-Viejo et al., 2012).

S2. Differences in crustal densities with regard to the previous model of Pedreira et al. (2007)

The density structure of the crust was taken mainly from the previous 3D model published by Pedreira et al. (2007). There are, however, some differences that will be described and discussed here.

Due to the limited vertical resolution of the code, the sedimentary layer in the Duero basin includes now the Cenozoic and the thin Mesozoic layer beneath it. The density of this cover varies from North to South. In the North, direct measurements in samples of both the Cenozoic and the Mesozoic gave an average value of 2460 kg m^{-3} (Evers, 1967). We have also included a body of dense conglomerates ahead of the mountain front with a density of 2600 kg m^{-3} . To the South, the more fine-grained sediments and the reduced thickness of the Mesozoic layers yield a lower average density, which we estimate to be $\sim 2300 \text{ kg m}^{-3}$ from the density-log of the Olmos-1 well (Location in Figure 2) (Gómez Ortiz et al., 2005).

The density of the pre-Mesozoic upper crust has been increased from 2670 to 2720 kg m⁻³. This was a requirement during the trial-and-error fitting of more observables than in the previous model, and it is justified because even though ~2670 kg m⁻³ is a good average of density determinations in samples collected at the surface (see Pedreira et al. (2007) and references therein), an increase in density with pressure at depth in the upper crust is to be expected, as pores and fractures close. The new value is also still within the dispersion range of experimental P-wave to density conversions. The density of the middle crust was also slightly increased from 2840 to 2860 kg m⁻³.

S3. Choice of thermal properties for the crust

S3.1. Thermal conductivities

Some measurements of thermal conductivities are available for the sediments of the Tertiary basins along oil exploration wells, summarized by Fernández et al. (1998). Six wells in the Tertiary sediments of the Duero foreland basin and 7 wells in the Mesozoic-Tertiary sediments of the North Iberian margin provided average values of 2.53 and 2.50 W m⁻¹ K⁻¹, respectively.

For the pre-Mesozoic upper crust, measurements are limited to 10 water and mining exploration wells in the Cantabrian and West Asturian-Leonese zones, providing a mean of 2.47 W m⁻¹ K⁻¹ for the upper ≤300 m (Fernández et al., 1998).

Deeper in the crust, uncertainties in the determination of the thermal conductivity greatly increase due to its dependence on composition, temperature and, to a minor extent, pressure. We made rough estimates on the average temperature of each crustal level based on the observed surface heat flow to calculate the conductivities, and then we used this information and other thermal properties to calculate the geotherm and

check for consistency. Experimental work at atmospheric pressures suggests that values between $1.80\text{-}2.20 \text{ W m}^{-1} \text{ K}^{-1}$ are appropriate for the temperatures and lithologies expected for the base of the upper crust ($\sim 275\text{-}300 \text{ }^\circ\text{C}$) (Vosteen and Schellschmidt, 2003). This number should increase, however, when taking into account the effect of pressure, which can rise the conductivity by $\sim 10\%$ at 0.5 GPa (Clauser and Huenges, 1995). We therefore assumed a thermal conductivity of $2.40 \text{ W m}^{-1} \text{ K}^{-1}$ for the pre-Mesozoic upper crust. According to the above-mentioned references and taking into account the combined effects of temperature and pressure, average values of 2.10 and $2.00 \text{ W m}^{-1} \text{ K}^{-1}$ were chosen for the middle and lower crust, respectively.

S3.2. Radiogenic heat production

Radiogenic heat production is assumed to be constant within each body of the model (Table 1). Cenozoic and Mesozoic sediments are assigned a volumetric heat production of $1.2 \text{ } \mu\text{W/m}^3$, which is the value determined by Brunet (1994) for sediments of this age in the eastern part of the Bay of Biscay.

For the pre-Mesozoic upper crust, we gathered heat production data determined in samples from the area (Fernández et al., 1998). The average value for three different lithologies of the Cantabrian Zone is $1.37 \text{ } \mu\text{W/m}^3$. The West Asturian-Leonese and Central Iberian zones, which are also present in the modeled transect beneath the sediments of the Duero basin (following the Cantabrian Orocline), yielded slightly higher values. Schists of the West Asturian-Leonese Zone provided an average value of $1.5 \text{ } \mu\text{W/m}^3$, whereas granites of this zone (very scarce, and more abundant in the vicinity of the Central Iberian Zone) yielded an average of $2.33 \text{ } \mu\text{W/m}^3$. The more granitic basement of the Central Iberian Zone, on the other hand, provided values of

2.45 $\mu\text{W}/\text{m}^3$ for the Spanish Central System and 2.36 $\mu\text{W}/\text{m}^3$ for the Toledo Mountains to the south (Jiménez-Díaz et al., 2012). Since we don't expect a large volumetric abundance of granitoids along the modeled transect, we have finally adopted the value of 1.65 $\mu\text{W}/\text{m}^3$, which represents a global upper crustal average according to Rudnick and Gao (2003).

For the middle crust, in absence of other sources of information, we have also chosen the worldwide average value proposed by Rudnick and Gao (2003), which is 1.00 $\mu\text{W}/\text{m}^3$.

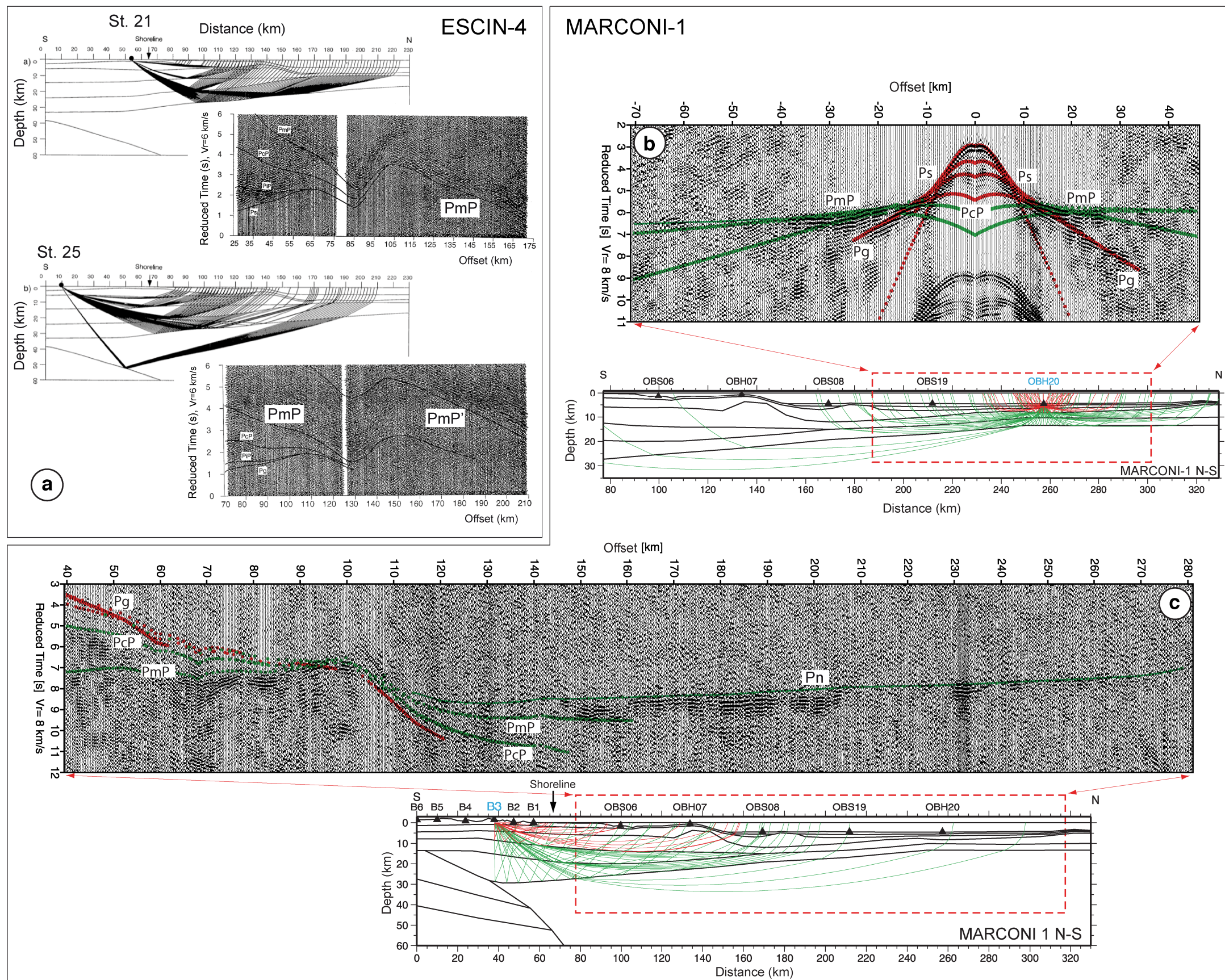
The lower crust was already divided in different bodies according to their relative proportions of felsic to mafic constituents (see section 4.3 of main article), which also control the relative abundance of heat-producing elements. Vilà et al. (2010) present an exhaustive analysis of heat production in many common lithological types and provide globally averaged values for lower crustal rocks of felsic-intermediate and mafic compositions, which are 0.50 and 0.15 $\mu\text{W}/\text{m}^3$, respectively. We have chosen values of 0.40 $\mu\text{W}/\text{m}^3$ for the southern part of the Iberian lower crust (ie. 70% felsic, 30% mafic) and 0.33 $\mu\text{W}/\text{m}^3$ for the subducting part located northwards (ie. 50% felsic-50% mafic). This last value was used as well for the European lower crust, except for the dense segment located beneath the thinnest part of the continental margin (HVLC), which is assumed to be essentially mafic and therefore a value of 0.15 $\mu\text{W}/\text{m}^3$ was used for it.

References

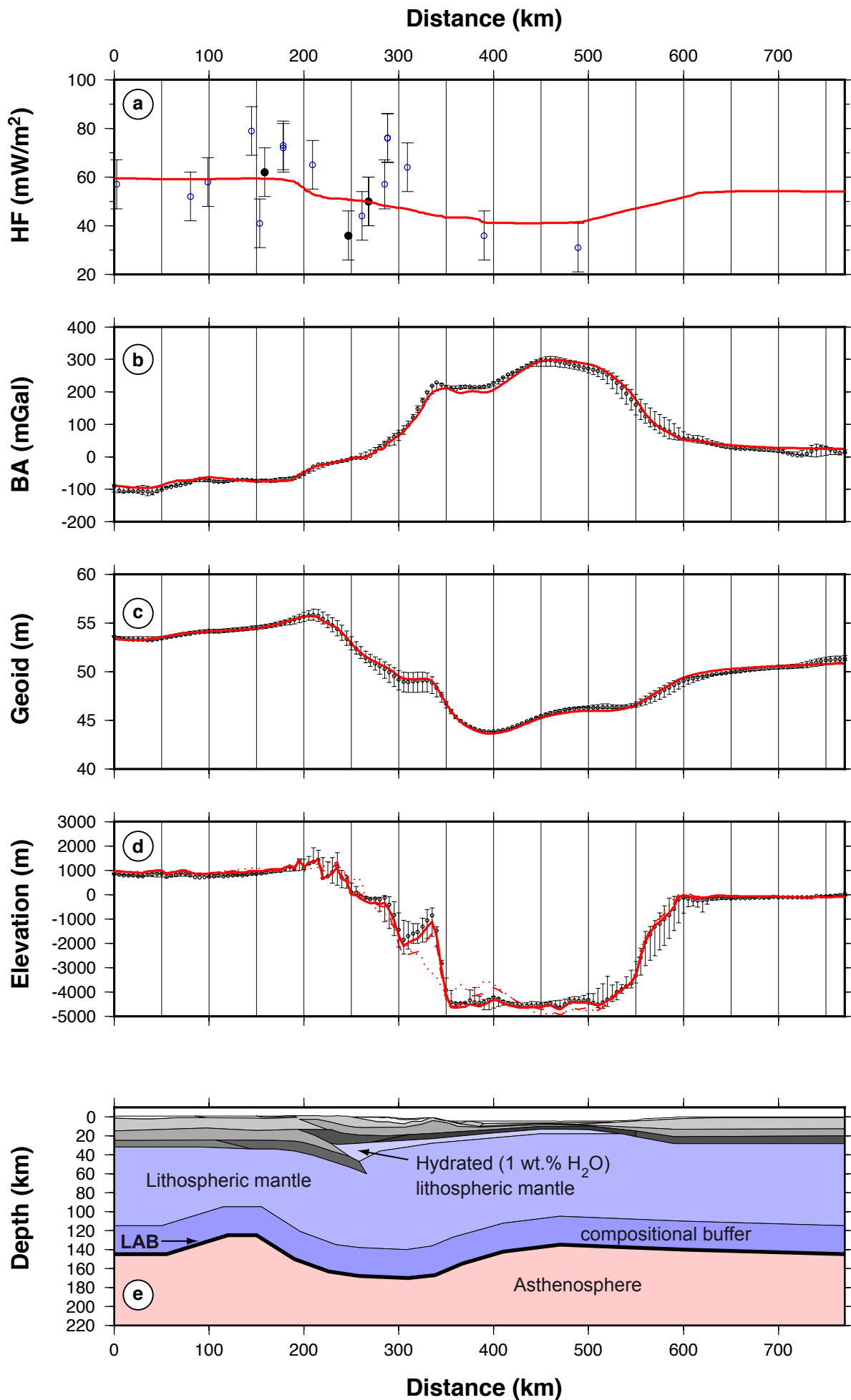
- Brunet, M.F., 1994. Subsidence in the Parentis Basin (Aquitaine, France): Implications of the thermal evolution, in: Mascle, A. (Ed.), *Hydrocarbon and Petroleum Geology of France*. Special Publication of the European Association of Petroleum Geologists, v. 4, Springer-Verlag, pp. 187–198.
- Cadenas, P., 2013, *Estructura geológica y modelización tridimensional de la*

- Plataforma Continental Noribérica entre 4° y 5°30 W (Golfo de Vizcaya), MSc Thesis, Univ. Oviedo, 47 pp.
- Clauser, C., Huenges, E., 1995. Thermal conductivity of rocks and minerals, in: Ahrens, T.J. (Ed.), *A Handbook of Physical Constants: Rock Physics and Phase Relations*. American Geophysical Union, pp. 105–126.
- Evers, H.J., 1967. Geology of the Leonides between the Bernesga and Porma rivers, Cantabrian mountains, NW Spain. *Leidse Geologische Mededelingen* 41, 83–151.
- Fernández, M., Marzán, I., Correia, A., Ramalho, E., 1998. Heat flow, heat production, and lithospheric thermal regime in the Iberian Peninsula. *Tectonophysics* 291, 29–53.
- Fernández-Viejo, G., Gallart, J., Pulgar, J.A., Córdoba, D., Dañobeitia, J.J., 2000. Seismic signature of Variscan and Alpine tectonics in NW Iberia: Crustal structure of the Cantabrian Mountains and Duero basin. *Journal of Geophysical Research: Solid Earth*, 105, 3001–3018.
- Fernández-Viejo, G., Gallart, J., Pulgar, J.A., Gallastegui, J., Dañobeitia, J.J., Córdoba, D., 1998. Crustal transition between continental and oceanic domains along the North Iberian margin from wide angle seismic and gravity data. *Geophys. Res. Lett.* 25, 4249–4252.
- Fernández-Viejo, G., Pulgar, J.A., Gallastegui, J., Quintana, L., 2012. The Fossil Accretionary Wedge of the Bay of Biscay: Critical Wedge Analysis on Depth-Migrated Seismic Sections and Geodynamical Implications. *The Journal of Geology* 120, 315–331. doi:10.1086/664789
- Gallart, J., Fernández-Viejo, G., Díaz, J., Vidal, N., Pulgar, J.A., 1997. Deep structure of the transition between the Cantabrian Mountains and the north Iberian Margin from wide-angle ESCI-N data. *Revista de la Sociedad Geológica de España* 8 (4), 365–382.
- Gallastegui, J., 2000. Estructura cortical de la cordillera y margen continental Cantábricos: Perfiles ESCI-N. *Trabajos de Geología* 22, 3–234.
- Gallastegui, J., Pulgar, J.A., Gallart, J., 2002. Initiation of an active margin at the North Iberian continent-ocean transition. *Tectonics* 21, 15–14.
- Gómez Ortiz, D., Tejero López, R., Babín Vich, R., Rivas-Ponce, A., 2005. Crustal density structure in the Spanish Central System derived from gravity data analysis (Central Spain). *Tectonophysics* 403, 131–149. doi:10.1016/j.tecto.2005.04.006.
- Heredia, N., Gómez, J.A., Molinero, R., León, C., Pineda, A., Delgado, B., Varea, R., Pulgar, J.A., Navas, M., 2010. Selección y caracterización de áreas y estructuras con capacidad de almacenamiento geológico de CO₂ en España, Vol I-1: Cadena Cantábrica y Cuenca del Duero (Geología). IGME, unpublished report (SID code: 64044), 113 pp.
- Jiménez-Díaz, A., Ruiz, J., Villaseca, C., Tejero, R., Capote, R., 2012. The thermal state and strength of the lithosphere in the Spanish Central System and Tajo Basin from crustal heat production and thermal isostasy. *Journal of Geodynamics* 58, 29–37. doi:10.1016/j.jog.2012.01.005.
- Pedreira, D., Pulgar, J., Gallart, J., Díaz, J., 2003. Seismic evidence of Alpine crustal thickening and wedging from the western Pyrenees to the Cantabrian Mountains (north Iberia). *J. Geophys. Res.* 108, B4, 2204. doi:10.1029/2001JB001667.
- Pedreira, D., Pulgar, J.A., Gallart, J., Torne, M., 2007. Three-dimensional gravity and

- magnetic modeling of crustal indentation and wedging in the western Pyrenees-Cantabrian Mountains. *J. Geophys. Res.* 112. doi:10.1029/2007JB005021.
- Pulgar, J.A., Gallart, J., Fernández-Viejo, G., Pérez-Estaún, A., Alvarez-Marrón, J., ESCIN Group, 1996. Seismic image of the Cantabrian Mountains in the western extension of the Pyrenees from integrated ESCIN reflection and refraction data. *Tectonophysics* 264, 1–19.
- Pulgar, J.A., Pérez-Estaún, A., Gallart, J., Alvarez-Marrón, J., Gallastegui, J., Alonso, J.L., Group, E., 1997. The ESCI-N2 deep seismic reflection profile: a traverse across the Cantabrian Mountains and adjacent Duero basin. *Rev. Soc. Geol. España* 8, 383–394.
- Rudnick, R.L., Gao, S., 2003. Composition of the continental crust, in: Rudnick, R.L., Holland, H.D., Turekian, K.K. (Eds.), *Treatise on Geochemistry*, Vol. 3: the Crust. Elsevier, Oxford, pp. 1–64.
- Ruiz, M., 2007, Caracterització estructural i sismotectònica de la litosfera en el domini Pirenaico-Cantàbric a partir de mètodes de sísmica activa i passiva. PhD Thesis, Univ. Barcelona, 354 pp.
- Ruiz, M., Díaz, J., Gallart, J., Pedreira, D., Pulgar, J.A., in prep., Seismic structure of the North-Iberian continental margin from wide-angle data of the MARCONI project.
- Vilà, M., Fernández, M., Jiménez-Munt, I., 2010. Radiogenic heat production variability of some common lithological groups and its significance to lithospheric thermal modeling. *Tectonophysics* 490, 152–164. doi:10.1016/j.tecto.2010.05.003
- Vosteen, H.-D., Schellschmidt, R., 2003. Influence of temperature on thermal conductivity, thermal capacity and thermal diffusivity for different types of rock. *Physics and Chemistry of the Earth, Parts A/B/C* 28, 499–509. doi:10.1016/S1474-7065(03)00069-X



Supplementary Figure 1. Record sections and raytracing modeling for some selected stations of the ESCIN-4 and MARCONI-1 seismic profiles, taken from Gallart et al. (1997) and Ruiz et al. (in prep.), respectively. **a)** Record sections of seismic stations 21 (close to the coast) and 25 (near the Duero basin), during the acquisition of the ESCIN-4 profile (see locations in Figure 2), and raytracing over the velocity model depicted in Figure 3. Thin lines on top of the record sections mark modeled arrival times. Observe that station 21 records a clear PmP reflection denoting a sharp interface at the base of the HVLC beneath Le Danois Bank and the continental platform, gently dipping towards the south. Station 25, on the other hand, records the presence of this same interface (Bay of Biscay Moho) as south as the coastline, as well as a later PmP' phase interpreted to be produced in the north-dipping Iberian Moho. **b)** Record section of Ocean Bottom Hydrophone OBH20 (the northernmost instrument along the MARCONI-1 profile) and raytracing through the final velocity depth model depicted in Figure 3 (only the marine sector of the model, where the airguns were shot, is shown here). Theoretical travel times and rays for P-waves propagating across the sediments and the upper crust are shown in red. Travel times and rays for waves propagating across deeper regions of the Bay of Biscay crust and upper mantle are shown in green. Ps, Pg and Pn denote refractions through the sediments, basement and upper mantle, respectively. PcP indicate reflections on top of the high-velocity lower crust. Note the clear Moho reflections (PmP) constraining the crustal thickness in this part of the margin. **c)** Record section of land station B3 during the acquisition of the MARCONI-1 profile, and raytracing through the velocity model of Figure 3. Same legend as in panel b. Note the strong Pn phase observed. With the depth and dipping of the Moho constrained by this and other instruments (eg. OBH20 in panel b), the arrival times of this Pn phase indicate relatively low P-wave velocities in the upper mantle of the North-Iberian margin (7.7-7.9 km/s; Figure 3).



Supplementary Figure 2. Same as Figure 5 but showing the fitting of observables for Model A extended 300 km farther north to incorporate the conjugate Armorican margin. (Continuation of Model B from 470 to 770 km is exactly the same as in this figure, with comparable fittings).